NASA CR-66759

DESIGN, FABRICATION AND EVALUATION OF TUNGSTEN ENCAPSULATED SILVER INFILTRATED POROUS TUNGSTEN ROCKET NOZZLE INSERTS

By Joseph Price

Prepared under Contract No. NAS 1-4722 by

ARDE-PORTLAND INC.
Paramus, New Jersey

for

NATIONAL AERONAUTICS AND SPACE ADMINISTRATION

TABLE OF CONTENTS

LIST OF ILLUSTRATIONS

LIST OF TABLES

ABSTRACT

This report covers the work performed to evaluate a self cooled rocket nozzle concept consisting of a silver impregnated tungsten throat insert designed to cool by evaporation of the silver coolant. The concept involves encapsulating a nozzle throat insert in a solid tungsten case with preselected vent regions to control the silver evaporation.

The reasoning leading to the concept is reviewed. The design, fabrication and testing of five experimental inserts are described. Two test inserts were unencapsulated and served as comparative controls to evaluate the performance of three encapsulated inserts. The encapsulated inserts differed from each other with respect to the encapsulation techniques used and/or the design of the coolant venting system.

The firing test conditions of the inserts are described. The description includes motor configuration and propellant gas properties. The results of each nozzle firing were evaluated and conclusion were drawn concerning the fabrication procedures and the design of subsequent nozzle inserts. A final conclusion is reached that the tests did not succeed in proving the validity of the encapsulation concept.

I - INTRODUCTION AND SUMMARY

The object of the investigation was to evaluate a silver impregnated tungsten nozzle concept self cooled by evaporation of the silver through specific vents provided in an encapsulating layer of dense tungsten.

Under Contract NAS 1-4722, Arde-Portland designed and fabricated five test rocket nozzles for the evaluation of nozzle throat inserts using such a cooling scheme. The inserts were expected to operate satisfactorily at flame temperatures of 6200-6800°F and chamber pressures greater than 500 psi for 60 seconds. The throat diameter of each nozzle insert was 1 1/4 inches.

Silver impregnated porous tungsten nozzle throat inserts have been investigated extensively and have been demonstrated with some success in rocket firings with gas temperatures of 6000°F and pressures of 600-900 psia. The actual performance, however, has not been as good as would be anticipated from the heat absorbing capacity of vaporizing silver. Arde-Portland felt that this performance short fall might be caused by the fact that the impregnated nozzle insert is exposed to the gas flow all along its gas side surface. The vaporization temperature of the coolant is thus a function of the local static pressure. As an illustration in a typical rocket motor with a chamber temperature of 6000°F and a chamber pressure of 800 psi the static pressure along a typical insert may vary from 640 psi at the upstream end to 240 psi at the downstream end. At 600 psi, silver vaporizes at 6100°F a temperature higher than the gas temperature so that there is no evaporative cooling of the upstream insert surfaces at all. Actually, a conventional silver impregnated

insert will be effective only where the local static pressure is low enough to permit the silver to vaporize at a temperature below the softening point of the tungsten matrix, about 5300°F. This pressure is 180 psia and will usually occur well downstream of the throat; thus the initial throat area is not helped.

To avoid this problem Arde-Portland proposed that the impregnated insert be coated with a thin impermeable layer of tungsten, except at preferred venting regions where the local static pressure would be consistent with a coolant vaporization temperature below the softening point of the tungsten. This type of insert is referred to as an encapsulated insert. Figure III-1 shows a cross section of the first encapsulated insert with vent holes in the cap, and Figure II-1 shows the insert assembled in a nozzle. Reference 1 provides a detailed discussion of insert encapsulation and preferential venting.

The intent of this program was to test silver impregnated tungsten nozzle throat inserts utilizing state-of-the-art techniques for encapsulating and venting. This approach was selected as one which would inexpensively establish the capability of current techniques, while readily identifying the areas requiring further development effort.

Arde-Portland designed and fabricated five (5) nozzles for test. The nozzles were identical except that the throat inserts varied as follows:

Insert #1: silver impregnated porous tungsten insert no encapsulation.

Insert #2: solid forged tungsten insert.

Insert #3: silver impregnated porous tungsten insert encapsulated in a plasma sprayed tungsten cap; vented.

Insert #4: silver impregnated porous tungsten insert encapsulated in a chemically deposited tungsten cap; vented.

Insert #5: silver impregnated porous tungsten insert encapsulated in a chemically deposited tungsten cap with longitudinal venting grooves between the tungsten cap and the impregnated tungsten substrate.

Nozzles 1 and 2 with unencapsulated inserts were used as controls for comparing the performance of the encapsulated inserts. Nozzles 3, 4 and 5 used variations of encapsulated inserts modified to obtain optimum performance. The five nozzles were fired under similar conditions except that the chamber pressure for Nozzle #3 was lower than for the others. This discrepancy was caused by problems with the test equipment.

Best Performance - Insert #4 Encapsulated impregnated insert.

2nd - Insert #1 Unencapsulated impregnated insert.

3rd - Insert #2 - Solid tungsten insert.

Encapsulated Insert #4 was best, marginally outperforming the unencapsulated impregnated Insert #1. The difference in performance, however, was small enough to be within the range of experimental error. Furthermore, examination of the fired Insert #4 indicated that the improved performance, if any, was not necessarily attributable to the encapsulation-preferential venting principle.

We must conclude that the value of the encapsulation-preferential venting principle has not been proven in practice. The anticipated mechanism of silver coolant migration to the vents from remote hot spots did not function.

II - DESIGN FIRING CONDITIONS AND NOZZLE CONFIGURATION

This section defines the firing conditions for which the Arde-Portland nozzle was designed and describes the nozzles and inserts as designed and fabricated. The five nozzles built and tested were identical except for the details of the throat insert.

II-1 Nozzle Geometry and Materials

A scale drawing of the nozzle is shown in Figure II-1. A conventional conical nozzle was chosen for simplicity, with a throat diameter of 1.25" and a throat radius of curvature of 1.25". The convergent cone half angle is 30° while the expansion cone half angle is 15°. The inlet diameter is 5.80" with a subscale approach area ratio of 21.5. The exit diameter is 4.76" which corresponds to an expansion area ratio of 14.5. For thermal purposes, a heat sink nozzle design was chosen using graphite as the heat sink material and silica phenolic and pyro-graphite as insulators. Graphite was used as the gas-side material due to its good chemical corrosion characteristics at high temperature. It was backed by silica phenolic which thermally protects the outer steel holding fixture (not shown) during firing and the subsequent cool down. To prevent longitudinal heat transfer into the test insert, pyro-graphite was used as an insulator instead of silica phenolic, since silica phenolic ablates excessively. During firing, the nozzle was attached to the rocket chamber by a cylindrical steel holding fixture. The rocket chamber and steel holding fixture were provided by the test facility.

NOZZLE CONFIGURATION, PREDICTED CORROSION & TEMPERATURE

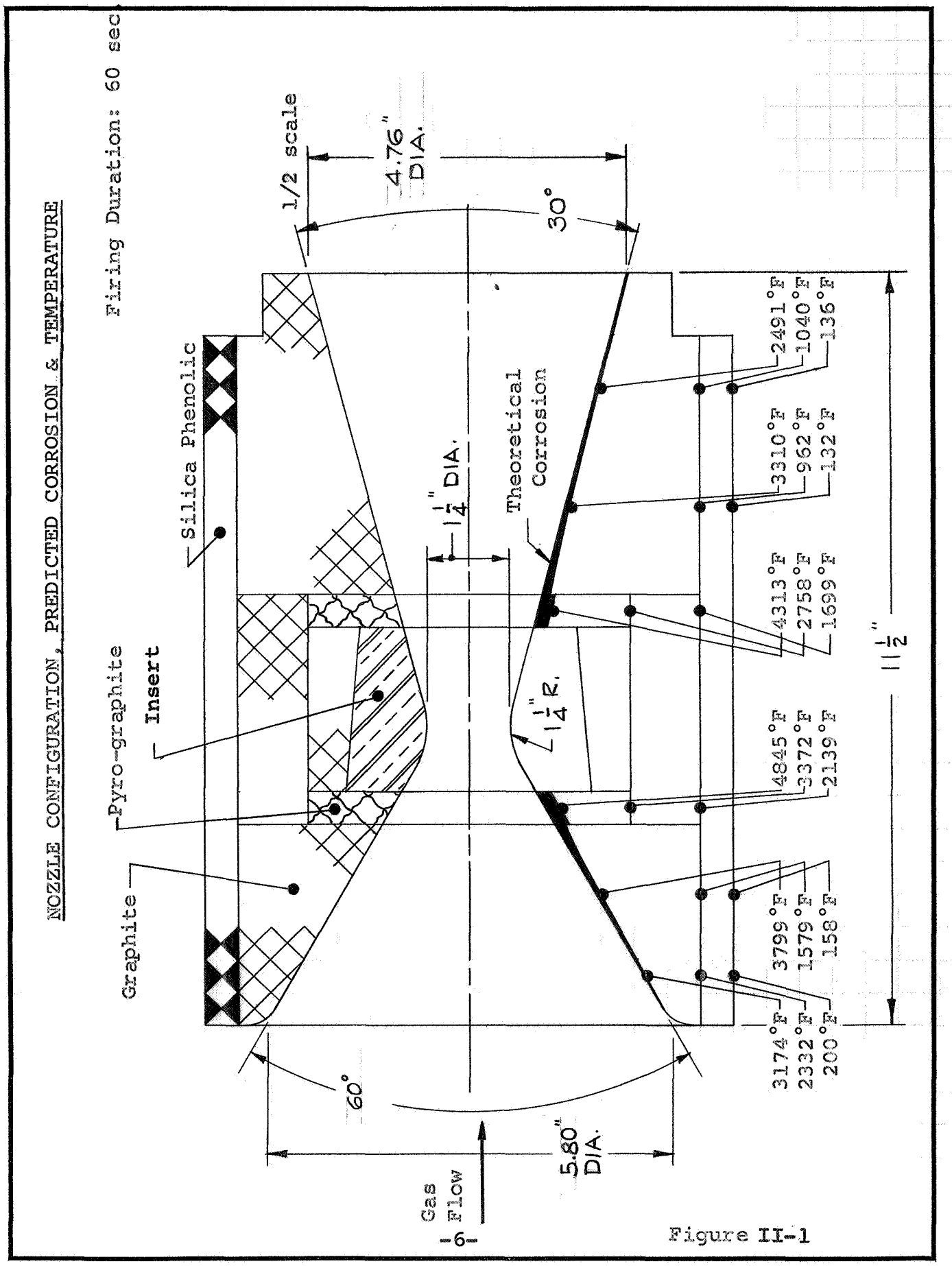

Figure II-1

II-2 Design Firing Conditions

The following nozzle design parameters were calculated assuming the use of United Technology Corporation UTP 3212 propellant with N_2O_4 oxidizer.

	PARAMETER	VALUE
1.	Chamber Temperature	6855°F
2.	Chamber Pressure	755 psia
3.	Firing Time	60 sec.
4.	Throat Diameter	1.25 inches
5.	Oxidizer Flow Rate	3.78 lb/sec.
6.	Fuel Flow Rate	2.36 lb/sec.
7.	Mass Flow Rate	6.14 lb/sec.
8.	O/F Ratio	1.6:1
9.	C*	5415 ft/sec.
10.	Exhaust Gas Composition:	

SPECIES	WT %
CO	34.509
CO_2	5.941
H_2	0.949
H	0.090
H_2O	6.305
N_2	19.025
O	0.032
OH	0.323
Al_2O_3	32.722

Specific heat ratio	1.179
Specific heat at constant pressure	0.3912 BTU/lb°F
Thermal conductivity	0.1998 BTU/hr. °F ft.
Viscosity	0.4294 lb/hr ft
Molecular Weight	33.49 lb/mole

Based on these characteristics, the heat transfer coefficients for the throat and the supersonic section of the nozzle were determined from Long's equation, while those for the subsonic section were determined from the Bartz's simplified equation. The heat transfer coefficient for the throat is 1674 BTU/hr $°F^2$ based on the C*, value of 5415 ft/sec.

The graphite saturation number, the amount of wall material which must be reacted with a unit mass of the combustion products to attain the equilibrium state at the wall temperature, for diffusion controlled chemical corrosion was determined from a simplified model based upon the following assumptions:

a. Complete thermodynamic equilibrium (kinetically limited reactions excluded from the analysis).

b. Diffusion due to thermal and pressure gradients is negligible compared to that due to concentration gradients normal to the wall.

c. All species diffusion coefficients are equal.

d. Prandtl and Lewis numbers are unity.

The results of the analysis gave a graphite saturation numbers of 0.06075 lb. of graphite per lb. of gas mixture. The theoretical corrosion at the end of 60 seconds of firing is shown on Figure II-1. The erosion depths computed should present no problems during the test since the calculation procuedure yields conservatively high results.

A thermal check of the nozzle was made for the expected conditions corresponding to the end of firing using a simplified one-dimensional constant-properties wall analysis. The temperatures of the critical components at the end of 60 seconds are shown on Figure II-1. The material properties for the various materials used in the analysis are shown in Table II-1. Temperatures other than the gas-side ones are conservatively high since cylindrical effects were neglected.

The temperatures shown do not present a problem since they are lower than those experienced in typical flight weight nozzles. The calculated gas-side temperatures of the materials are low and indicate that corrosion will not be entirely diffusion controlled and kinetic reactions will prevail throughout the major portion of the firing time.

TABLE II-1

MATERIAL PROPERTIES FOR SIMPLIFIED WALL ANALYSIS

Material	$\bar{T}$	k	ρ	c	ρc	α
	°F	$\frac{BTU}{hr\ °F\ ft}$	$\frac{lb}{ft^3}$	$\frac{BTU}{lb\ °F}$	$\frac{BTU}{ft^3 °F}$	$\frac{ft^2}{hr}$
Pyro-graphite"ab"	2500	58.0	138	0.402	55.5	1.045
Pyro-graphite "c"	2500	0.66	138	0.402	55.5	.01189
Graphite HLM	2000	24.2	108	0.463	50.0	.4840
Silica Phenolic	1000	0.18	110	0.2245	24.7	.007287

III - DESIGN, FABRICATION AND TEST OF PLASMA SPRAY ENCAPSULATED THROAT INSERT #3

III-1 Design and Configuration of Insert #3

The first insert fabricated and tested is identified as Insert #3. The test insert shown in Figure III-1 consists of an 80% tungsten 20% silver filled matrix completely encapsulated in a tungsten cap approximately 0.060" thick. The assay sheet of the infiltrated inserts provided by the vendor is shown in Table III-1. Prior to discussing the thermal and venting aspects of the encapsulated insert, several paragraphs on the encapsulation modes considered, and the one finally utilized in the test insert configuration, will be presented.

III-1.1 Encapsulation Methods

The prime purpose of encapsulation was to achieve an adherent, dense, impermeable, coating of tungsten to coat the silver impregnated tungsten insert material on all surfaces and to permit establishment of controlled venting of the coolant.

It was believed that theoretical density and hence impermeability could be achieved by a chemical deposition process utilizing the reduction of tungsten carbonyl or tungsten hexafluoride. This approach was initially pursued, but the coating vendor was unable to deposit more than a few

TEST INSERT CONFIGURATION

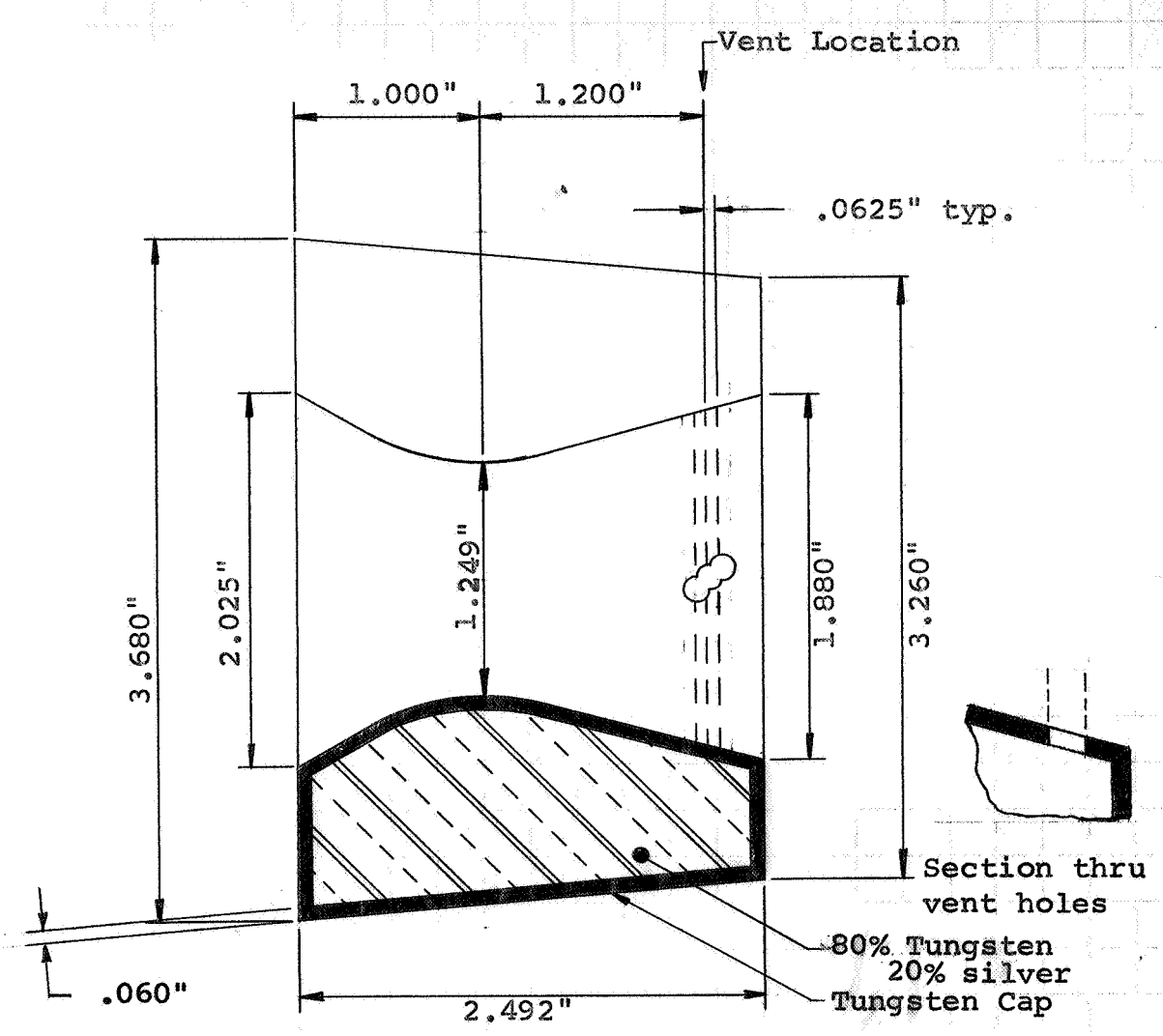

Vent Location

1/8" dia. vent holes
54 holes (18 holes per circle)
0.075" depth from 0-180°
0.125" depth from 180-360°

WAH CHANG CORPORATION
ALBANY DIVISION

Lot	Dimensions	Weight
7939-1	1 pc 3.758" x 1.246" x 2.532"	15.6 lbs.
7939-2	1 pc 3.758" x 1.246" x 2.516"	15.5 "

TUNGSTEN POWDER LOT NUMBER
C20-147, WCC
ANALYSIS IN PERCENT

Al	<.001
C	<.003
Cb	<.010
Cr	<.001
Cu	<.001
Fe	<.002
Mn	<.001
Mo	.005
Ni	.001
O	.048
Si	<.001
Ta	<.005
Ti	<.002

SILVER LOT NUMBER 3-3-65
Engelhard
ANALYSIS IN PERCENT

Al	<.003
C	<.003
Cr	<.001
Cu	.078
Fe	.018
Mn	<.001
Mo	<.001
Ni	<.001
O	<.001
N	<.0005
Ni	<.001
Si	.119
Ti	<.002

SINTERED DENSITY
78.5 Percent of Theoretical

SILVER INFILTRATION
Greater Than 90 Percent of Pores Filled

ULTRASONIC INSPECTION
Acceptable, No Rejectable Indications

DYE PENETRANT INSPECTION
Acceptable, No Rejectable Indications

TABLE III-1

thousanths of an inch of tungsten instead of the desired thickness of 0.060". An alternate coating method, plasma deposition, was undertaken. Tungsten coatings achieved by atomizing tungsten powder and using a plasma flame as a heat source do not result in near theoretical density. The best densities (90-95%) have been obtained by controlled atmosphere deposition within an environmental chamber. This method of operation is only practical when substrate temperatures are allowed to exceed 2000°F and when the hardware is of simple geometry so that deposition can be accomplished normal to the coating surface. When the part includes angles, converging and diverging areas as in the case with the insert under discussion, intricate tooling and mechanization are required to conduct deposition normal to all surfaces. Moreover, the presence of silver which melts at 1762°F, does not allow high temperature deposition. For these reasons spraying was done under open air conditions. Based on extensive past experience such deposition results in an as sprayed density on the order of 80-90% of theoretical density. The smaller density figure applies in the critical throat areas, since it is there that deposition angles deviate appreciably from 90°. The higher density approaching 90% of theoretical, exists on the less critical external diameter surfaces where it is simple to maintain a spray stream normal to the substrate. The "stand-off" or torch to work distance also affects density with higher density

being commensurate with stand-off distances of less than 6 inches. A distance of 2-4 inches was maintained during deposition. Though argon was used as the plasma forming, powder carrier and cooling gas, a small amount of tungsten oxide was entrained in the coating. The oxide content lowers the cohesive strength of the particle to particle bonding.

III-1.2 Vent and Thermal Considerations

Before the vapor vent location can be determined the silver properties must be determined. The basic silver properties used are as follows:

Density	656 lb/ft^3
Melting Point	1762°F
Latent Heat of Fusion	40 BTU/lb.
Boiling Point at Atmospheric Pressure	3952°F
Latent heat of Vaporization	1016 BTU/lb.

The nomenclature used in the remainder of Section III-1.2 is listed below:

P_v = vapor pressure of silver lbs/ft^2 absolute
T_v = temperature of silver °R
Log P_v = logarithm to base 10 of P_v
T_c = critical temperature of silver °K
T_{NB} = boiling temperature of silver at atmosphere pressure °K
T_{v1} = a temperature °K
L_{v1} = latent heat of vaporization of silver at temperature T_{v1} BTU/lb
T_{v2} = another temperature °K
L_{v2} = latent heat of vaporization of silver at temperature T_{v2} BTU/lb

The vaporization pressure as a function of vaporization temperature, Figure III-2, was obtained by the following equation:

$$\text{Log } P_v = 8.79 - \frac{24,400}{T_v}$$

The critical temperature of silver was estimated by the equation of Gates and Thodas:

$$T_c = 1.4732\ (T_{NB})\quad 1.0313$$

with temperature in °K. The latent heat of vaporization, Figure III-2 was estimated by Watson's correlation:

$$\frac{L_{v2}}{L_{v1}} = \frac{T_c - T_{v2}}{T_c - T_{v1}}$$

where condition 1 was taken at the atmospheric boiling point.

The vapor vent location was determined by setting the vaporization temperature at the vent equal to 4750°F which corresponds to a vaporization pressure of 89.09 psia or a pressure ratio of 0.118. Pressure ratio as a function of axial length shown in Figure III-3 indicates the vent location is 1.20" down-stream of the throat (Figure III-3). The vent consisted of 54 holes of 1/8" diameter which provided 52% vented area at this location.

While preliminary indications were entirely favorable the configuration and size of the encapsulated impregnated throat insert matrix impose restrictions on the vapor flow dynamics which require closer scrutiny. An analysis related to flow

LATENT HEAT OF VAPORIZATION AND VAPORIZATION PRESSURE VERSUS VAPORIZATION TEMPERATURE FOR SILVER

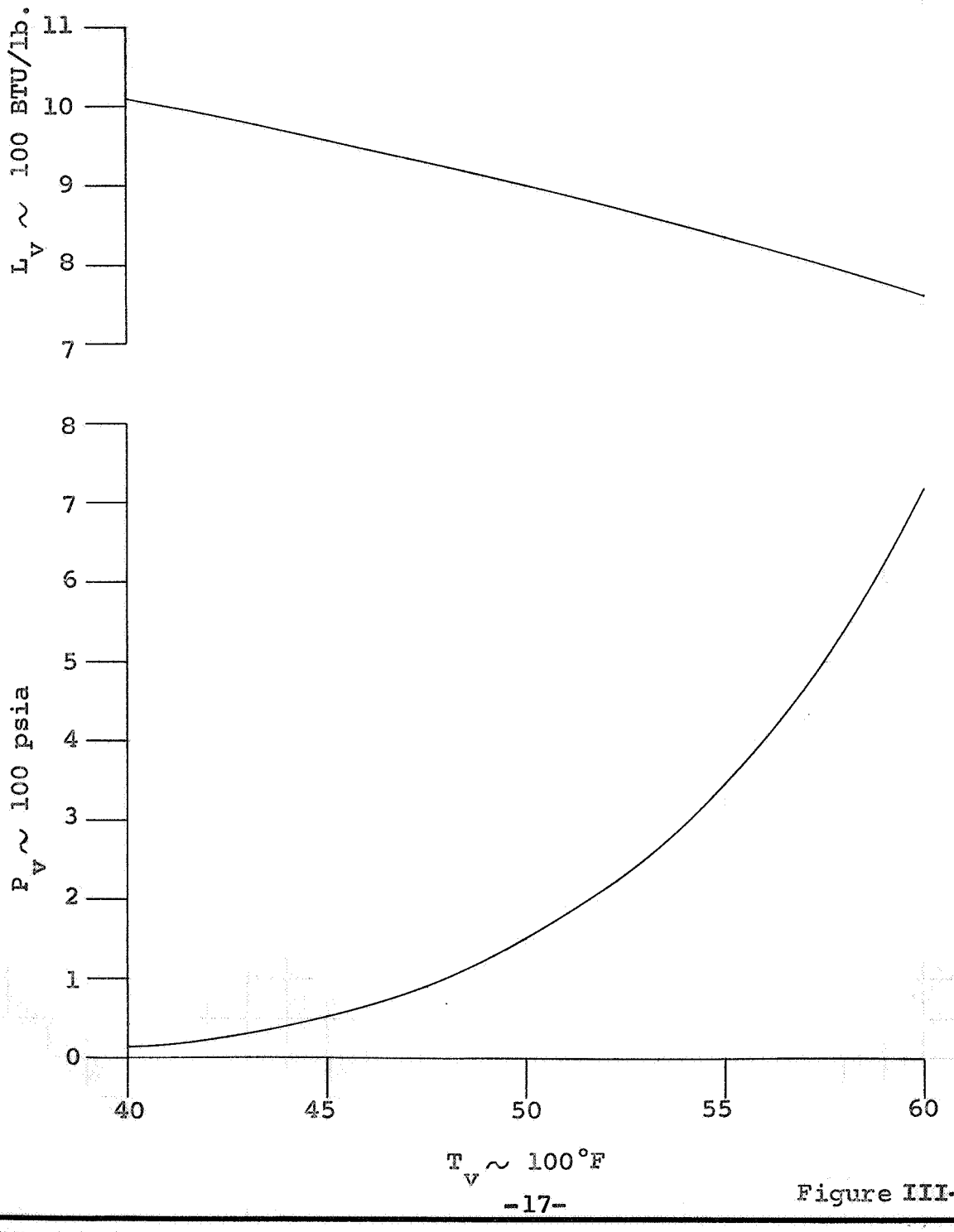

Figure III-2

SUPERSONIC PRESSURE RATIO VERSUS DISTANCE FROM THROAT

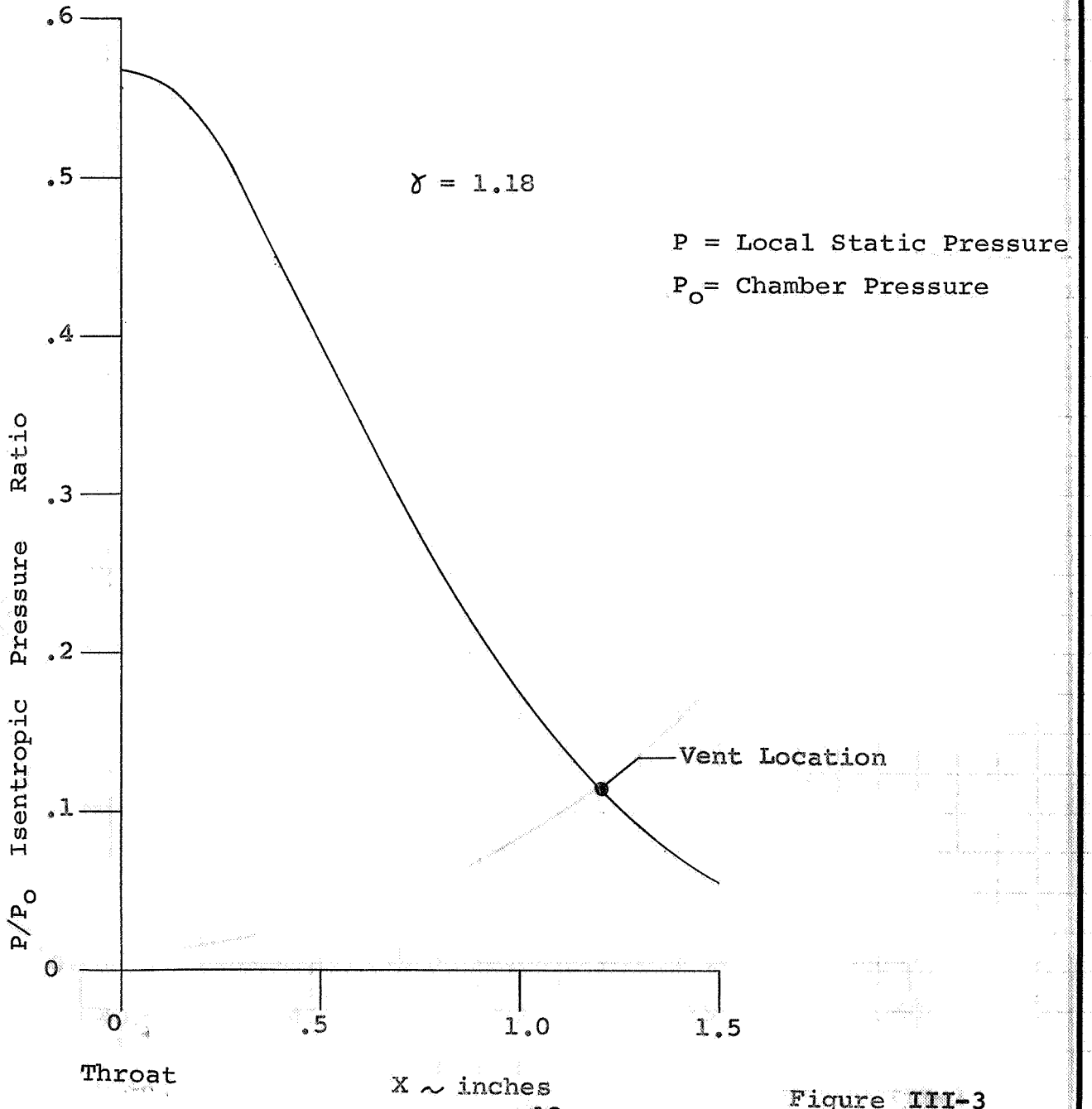

Figure III-3

and venting of the impregnant, was not carried out because of the obvious complexity in performing a rigorous analysis. However, a preliminary analysis made in accordance with the principles presented in Appendix B of ARDE-PORTLAND Proposal P-3116A to NASA-LRC was utilized to estimate the pressure distribution within the matrix. Appendix B of ARDE-PORTLAND Proposal P-3116A is reproduced in this report as Appendix 1. Flow, heat flux, venting and pressure drops were all taken into account in the estimate. The internal insert matrix pressure in the throat region was estimated to be 150 psia which corresponds to a vaporization temperature of 5000°F.

A one dimensional thermal analysis was performed on the nozzle throat cross section using a numerical method described in Appendix 2. The calculation is considered one dimensional since heat flow is assumed to be in the radial direction only. Tangential heat flow is assumed to be zero and heat flow parallel to the nozzle axis is assumed to be negligible. See Appendix 2 for a description of the procedure. The results are shown in Figure III-4. The various material properties, Table III-2, were considered invariant with time. In general, the theoretical results indicated sufficient impregnant was available to permit successful operation of the insert if the evaporative process cooled the insert cap as postulated.

TEMPERATURE HISTORY AT THROAT SECTION OF NOZZLE

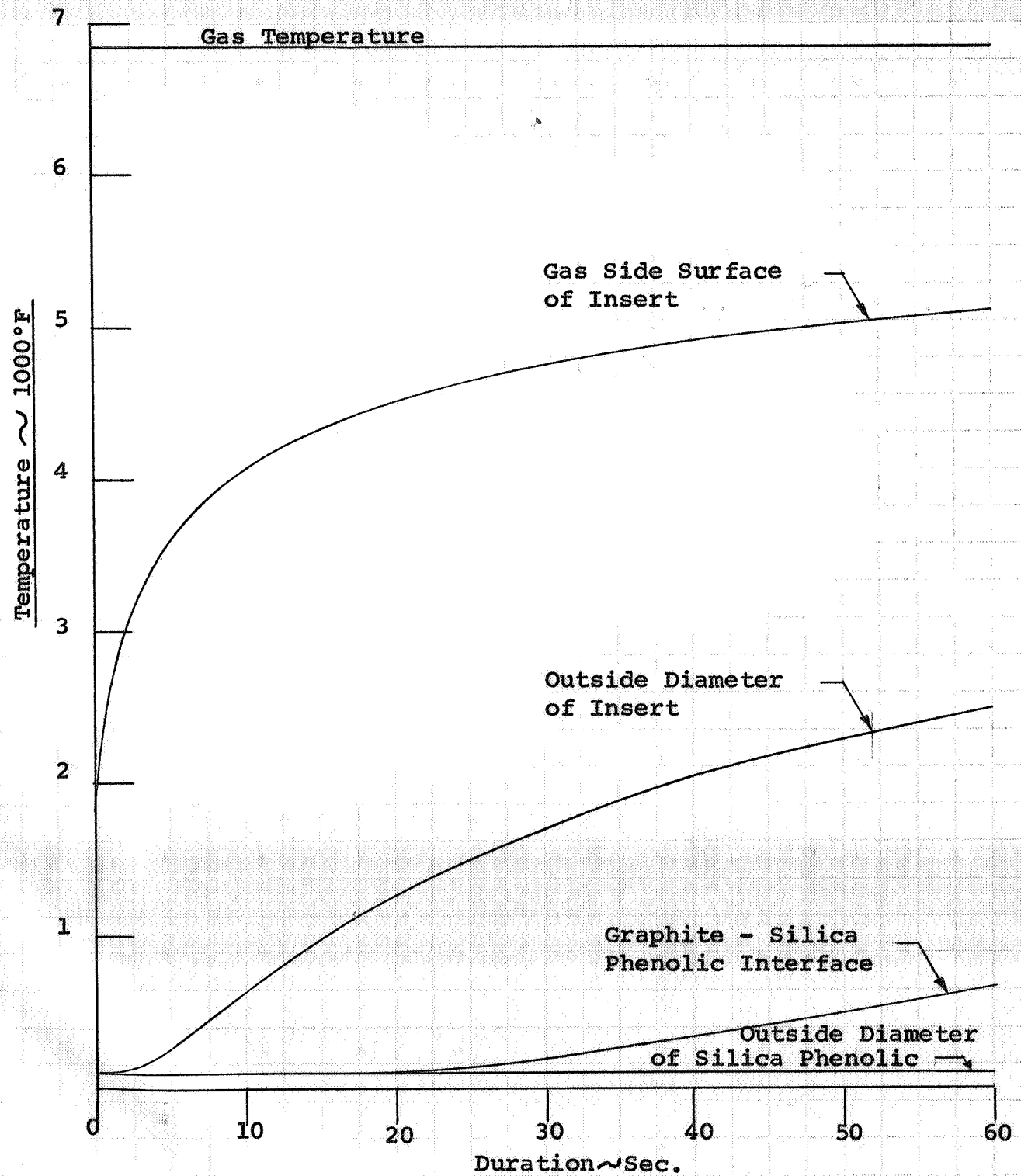

Figure III-4

TABLE III-2

MATERIAL PROPERTIES

Material	$\bar{T}$	k	ρ	c	ρc	α
	°F	$\frac{BTU}{hr\ °F\ ft}$	$\frac{lb}{ft^3}$	$\frac{BTU}{lb\ °F}$	$\frac{BTU}{ft^3\ °F}$	$\frac{ft^2}{hr}$
Tungsten	2500	62.5	1204	0.0382	46.0	1.359
80W-20Ag	2500	46.7	1094	0.050	54.7	.8537
Graphite	1500	28.1	108	0.440	47.5	.5916
Silica Phenolic	300	0.17	110	0.30	33.0	.005152

III-2 Actual Firing Conditions for Nozzle with Insert #3

The actual test parameters shown in Table III-3, were obtained from United Technology Corporation Report No. 2152-FR entitled "HTM-18 Nozzle Test Firing". HFX-6357 propellant was used with N_2O_4 as an oxidizer. The calculated chamber temperature is 6700°F. Actual chamber pressure was 500 psia and the gas properties are as follows:

Specific heat ratio	1.181
Specific heat at constant pressure	0.3950 BTU/lb°F
Thermal conductivity	0.2008 BTU/hr°F ft.
Viscosity	0.4367 lb/hr. ft.
Molecular weight	32.83 lb/mole

The gas properties are substantially the same as those for the design condition (See Section III-1.2).

The throat heat transfer coefficient was calculated to be 1604 BTU/hr°F ft^2 based on a mass flow rate of 5.16 lb/sec. This value is also basically the same as that for the design condition.

The graphite saturation number is 0.09005, an increase of 48% over the design condition. Although the graphite saturation number increased, the graphite corrosion at 60 seconds for the design condition is basically equal to the graphite corrosion at 39.65 seconds for the test condition,

TABLE III-3

NOZZLE TEST PARAMETERS

	PARAMETER	VALUE
1.	Chamber Temperature	6700°F
2.	Chamber Pressure	500 psia
3.	Firing Time	39.65 sec
4.	Throat Diameter	1.249"
5.	Wox	3.19 lb/sec
6.	Wfuel	1.97 lb/sec
7.	Mass Flow	5.16 lb/sec
8.	O/F ratio	1.6:1
9.	Exhaust Gas Composition	

SPECIES	MOLES/100 GRAM
CO	1.2020
CO_2	.1414
H_2	.4687
H	.1295
H_2O	.3794
O_2	.0018
O	.0055
OH	.0308
N_2	.6832
NO	.0037
Al_2O_3	.3168

due to the reduction in firing time. The corresponding tungsten saturation number is 0.3462 which gives a calculated corrosion rate of 4.8 mil/sec at the throat.

Due to the reduction in chamber pressure from the design to test condition, the calculated vent pressure was approximately 59 psia; the vaporization temperature 4560°F. The throat section matrix pressure is calculated to be approximately 120 psia which corresponds to a vaporization temperature of 4900°F. The temperature history shown in Figure III-4, up until 40 seconds, will still apply for the test condition but will be conservative since Figure III-4 was developed for a higher gas temperature.

III-3 Test Techniques and Results

The nozzle with Insert #3 was fired June 16, 1965. The results of the test are discussed in next few paragraphs.

III-3.1 Motor Configuration

A two segment HTM-18 hybrid gas generator per United Technology drawing 7300-208 was used for this test. A graphite mixer section (UTC drawing 7300-178) was placed aft of the solid fuel to insure complete mixing and combustion of the propellant gases prior to entering the nozzle area. The mixer throat diameter was 3.75 inches. (Reference UTC 2152-FR).

III-3.2 Propellant Description

The solid fuel used was formulation HFX-6357, containing 45% aluminum and 55% binder by weight. The binder consisted of polybutadiene acrylonitrile (PBAN), DER 332, and methyl nadic anhydride (MNA). The standard HTM-18 six-point star mandrel (UTC drawing 7300-18) was used for the solid fuel shape. The initial fuel perforation perimeter was 70 inches with an initial port area of 58 sq. inches. The total fuel length was 58 inches.

Nitrogen tetroxide (N_2O_4) used as the oxidizer was injected into the combustion chamber through one spray injector at a flow rate of 3.19 lbs/sec.

Ignition of the motor was achieved by injecting methylhydrazine (CH_3, NH, NH_2) into the combustion chamber at a flow rate of 0.50 lbs/sec. for 1.65 seconds at the beginning of the test. (Reference UTC 2152-FR).

III-3.3 Firing Data

The following test data were obtained:

Throat Diameter (Pre-Fired)	1.249 inches
Throat Diameter (Post-Fired Nominal)	1.563 inches
Burn time	39.65 seconds
Initial Chamber Pressure (Nominal)	580 psig
Final Chamber Pressure (Nominal)	395 psig
Burn time for 21% Drop in Chamber Pressure from 580 psig to 455 psig	29.3 seconds

III-3.4 Post Fired Nozzle and Insert Analysis

Examination of the fired nozzle showed that all of the nozzle was in good condition except the nozzle insert. Examination of the silica phenolic holder upstream and downstream, indicates little or no thermal penetration during heat soak. The pyrolytic graphite washers and the graphite exit cone were reusable and any erosion incurred was uniform. Erosion of the graphite cone section was negligible. There was a deposition of metallic slag in the upstream section of the exit cone. A sample of this slag was removed and the metallographic analysis indicated it was tungsten and silver. The tungsten-silver was probably carried by the gas boundary layer from the eroding throat insert and deposited downstream on the cooler graphite exit cone surface.

Post fire inspection showed that all of the plasma sprayed tungsten coating on the gas side of the nozzle insert was gone. The pressure trace shows that after the initial ignition peak, the nozzle operated stably for about 12 1/2 seconds at which time the pressure began to fall off steadily indicating steady erosion of the nozzle throat. At the end of 29.3 seconds, the chamber pressure had dropped 21% and shortly thereafter the firing terminated. Figure III-5 shows the firing pressure trace.

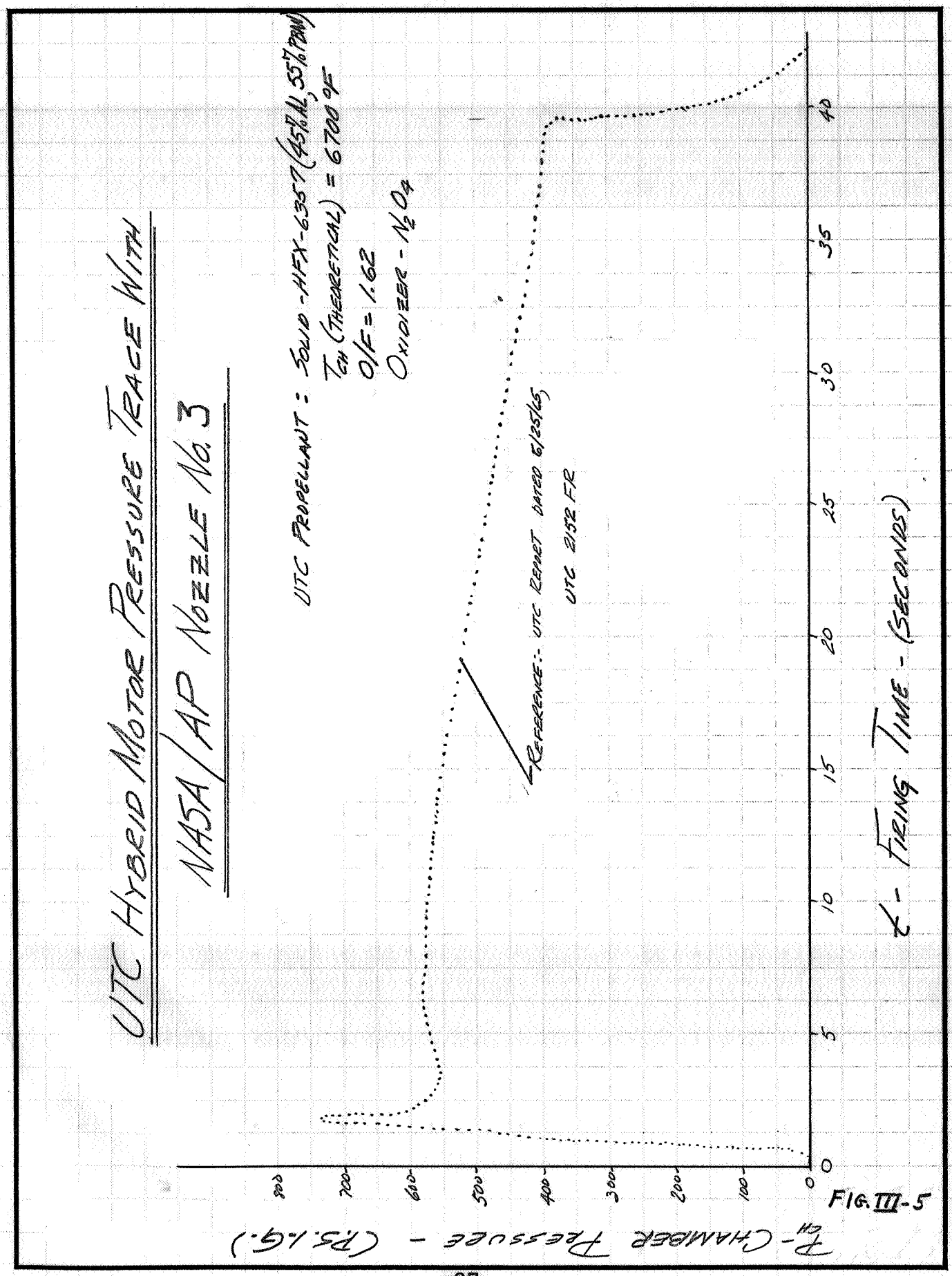
UTC Hybrid Motor Pressure Trace With
NASA/AP Nozzle No. 3
UTC Propellant : Solid-HFX-6357 (45% AL, 55% PBAN)
T_{CH} (Theoretical) = 6700 °F
O/F = 1.62
Oxidizer - N_2O_4
Reference:- UTC Kennet dated 6/25/65,
UTC 2/32 FR
P_{CH} - Chamber Pressure - (P.S.I.G.)
t - Firing Time - (Seconds)
0
100
200
300
400
500
600
700
800
5
10
15
20
25
30
35
40

FIG. III-5

Figure III-6 presents a half scale section of the nozzle with measured erosion depths. The erosion experienced by the major portion of the nozzle was extremely mild and the only area of substantial erosion was the insert. Figure III-7 presents full scale critical post fired insert flow areas. The erosion is generally uniform except for the gouge in the throat section. Tables III-4 and III-5 summarize the erosion rates and area changes of the critical nozzle components. The erosion rates in Table III-4 are based on a web time of 39.65 seconds, and were applicable on a web time of 27.15 seconds which is based on the indicated constant throat area shown in the pressure trace Figure III-5. Erosion rate for the throat section based on a 27.15 sec. web time was 5.78 mils/sec. for an area increase of 56.6%. The upstream pyrolytic washer eroded at about 3.0 mils/sec. whereas the downstream pyrolytic washer eroded only 0.4 mils/sec. This small erosion rate downstream of the insert was probably due to the reduced external heat input and the insulated effect of the carry over tungsten-silver slag. The excessive erosion of the tungsten capped infiltrated insert was due to the low strength of the plasma sprayed cap and possibly poor adherence of the cap to the substrate. Poor adherence would increase the thermal resistance between the cap and the substrate causing the cap gas side surface to reach diffusion controlled erosion temperature very early in the firing schedule thus increasing the erosion.

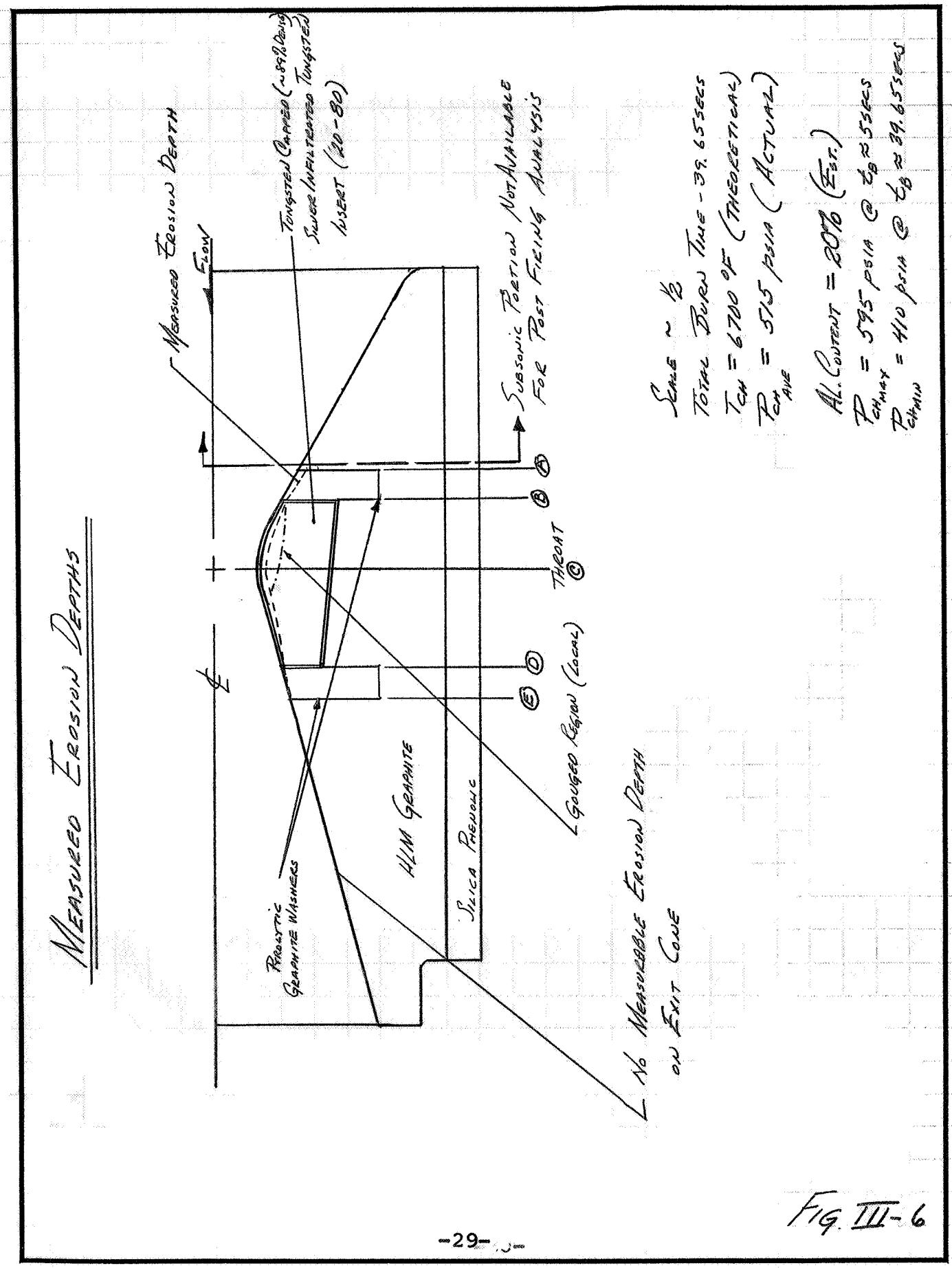

MEASURED EROSION DEPTHS

FIG. III-6

CRITICAL POST FIRED INSERT FLOW AREAS

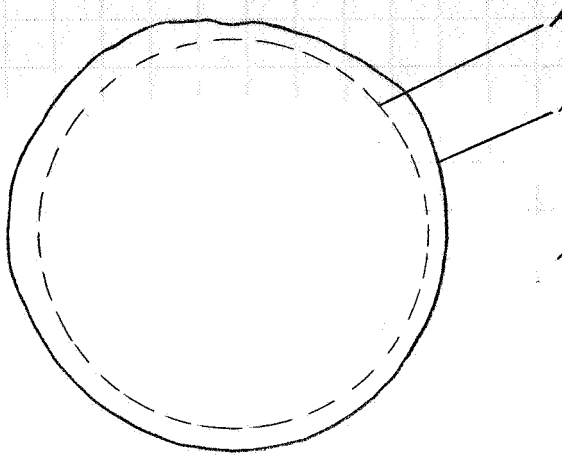

APPROACH SECTION-Ⓑ

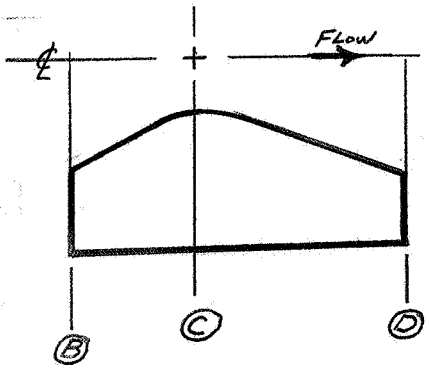

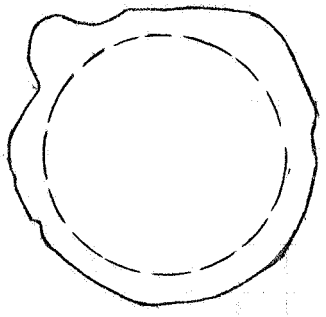

THROAT SECTION-Ⓒ

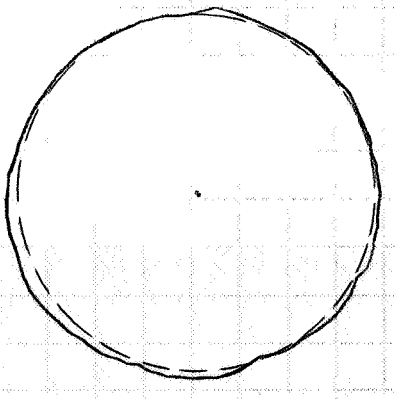

EXIT SECTION-Ⓓ

FIG. III-7

Erosion Rate Summary

Description	Section	Erosion Rate (Linear) Based on t_B=39.65 secs	Based on t_B=27.15 secs (Where Applicable)	Remarks
Upstream "Pyro"	A	3.66 Mils/sec	NA	Uniform Erosion on
" " "	B	2.52 Mils/sec	NA	Entire Washer
Insert-W-Ag	B	3.75 Mils/sec	5.47 Mils/sec *	Approach Section
with W Cap	C	3.96 Mils/sec	5.78 Mils/sec *	Throat Section
" " "	C	4.72 Mils/sec	6.90 Mils/sec *	Throat Section (Gouged Region)
" " "	D	0.69 Mils/sec	1.01 Mils/sec *	Exit Section
Downstream "Pyro"	D	0.76 Mils/sec	NA	Uniform Erosion on Entire
" " "	E	Negligible	NA	Washer
Graphite Exit	E	Negligible	NA	No Measureable Erosion
Cone	Etc	~ 0	NA	on Entire Exit Cone

*- Based on Pressure Trace which indicates Essentially Constant Pressure for First 125 secs.

Table III - 4

Percent Increase in Local Areas

Description	Section	% Increase in Area
Upstream "Pyro"	A	23.5
" " "	B	21.0
Insert-W-AG	B	31.4
with WCap	C	56.6
" " "	D	5.8
Downstream	D	6.5
"Pyro"	E	Negligible
Graphite Exit	E	≈0
Cone	etc	

Table II-5

The early wiping off of the tungsten cap surface did not allow evaluation of the canned insert concept.

The fired insert was cut in several places (see Figure III-8) and microspecimens made of the sections considered pertinent. In general, the microstructures confirm the visual observations of the post fired nozzle and nozzle insert, namely the insert was not permitted to operate in the preferential vented mode since the low density plasma sprayed tungsten cap was wiped away early in the firing. Because of the early loss of the tungsten cap, the encapsulation concept cannot be evaluated from this test.

III-4 Conclusions from Firing of Nozzle with Insert #3

a. The ARDE-PORTLAND nozzle is adequate for the testing of the nozzle inserts under the prescribed conditions.

b. A cap of low strength plasma sprayed tungsten does not provide an adequate structure to permit evaluation of the concept of an encapsulated impregnated nozzle.

c. The infiltrated matrix operated essentially as a conventional impregnated insert due to the loss of the tungsten cap early in the firing. The erosion rate based on a linear burn time was 4 mils/sec.

MICROSPECIMEN LOCATIONS

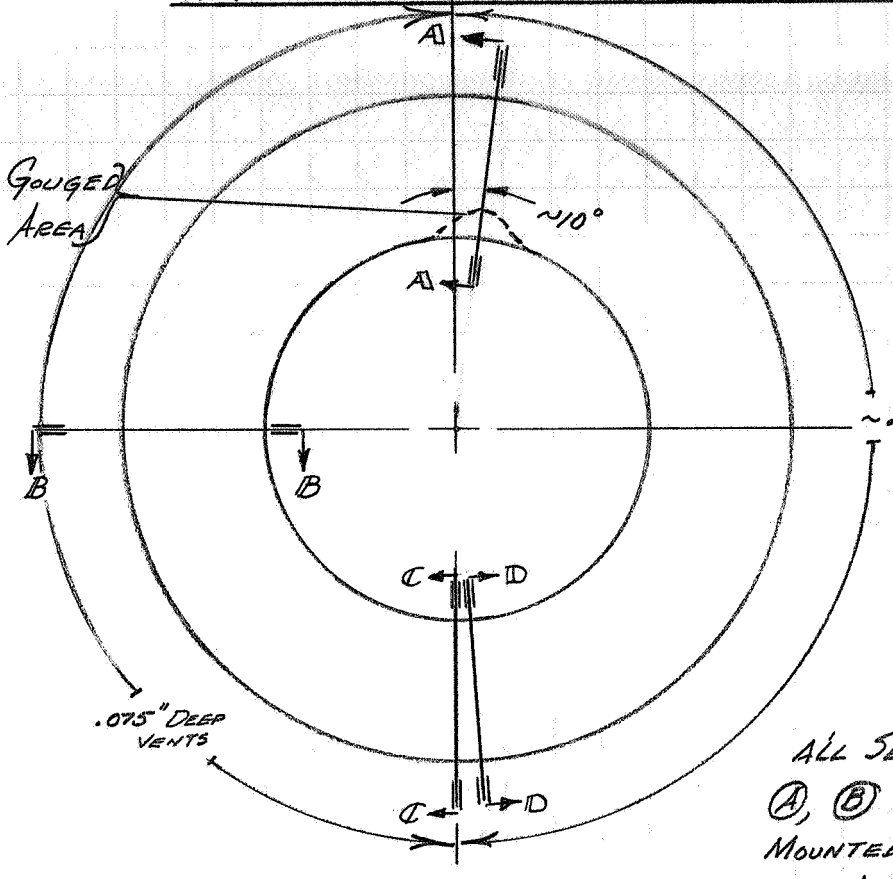

ALL SECTIONS SHOWN IN (A), (B) AND (C) WERE MOUNTED FOR METALLOGRAPHIC ANALYSES. SECTION (D)-(B) WAS CUT FOR CHEMICAL ANALYSIS

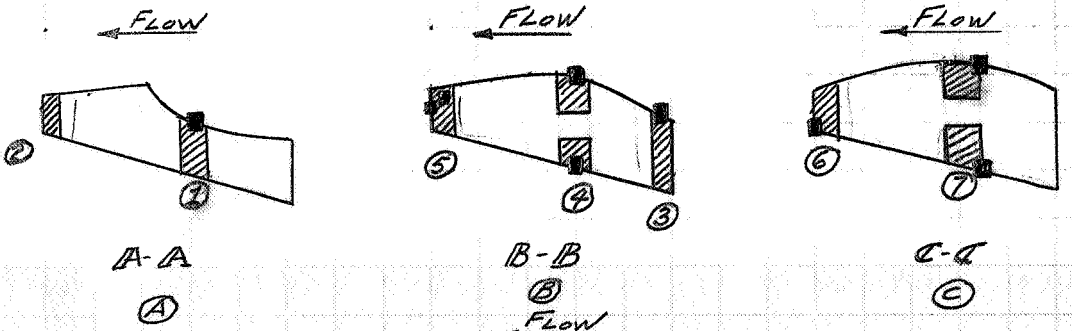

■ - MICROSTRUCTURE SHOWN IN FOLLOWING FIGURES

FIG. III-8

d. Microstructures of the post fired insert indicate little silver depletion throughout the tungsten matrix.

e. The preferential venting characteristics of the insert were not exploited because of premature wiping off of the cap.

f. The other nozzle components were in reusable condition including the silica phenolic nozzle holder.

g. To obtain a meaningful test of the encapsulation concept, the insert cap should be fabricated of high density tungsten (greater than 98%) and be continuous over the I.D., O.D. surfaces, and downstream and upstream faces.

h. The performance of the encapsulated insert should be judged against the performance of a solid forged tungsten insert and an unencapsulated silver impregnated tungsten insert, all fired under similar conditions. To accomplish this a vendor capable of plating high density tungsten in the required thickness must be searched for and located.

IV - DESIGN FABRICATION AND TEST OF NOZZLES WITH INSERTS #1, #2 and #4

IV-1 Design and Description of Inserts

In accordance with the conclusions given in Section III-4 and in coordination with Langley Research Center the next effort consisted of the design, fabrication and testing of the following nozzle inserts:

Insert #1 - silver impregnated porous tungsten - no encapsulation

Insert #2 - solid forged tungsten insert

Insert #4 - silver impregnated porous tungsten insert encapsulated in a chemically deposited dense tungsten coat

These inserts were the same size and shape as Insert #3 previously discussed except that no venting holes were made for Insert #1 because it was not encapsulated, nor for Insert #2 since it was not impregnated.

Inserts #1 and #2 served as datum configurations for evaluating the encapsulated Insert #4 to determine whether encapsulation had substantially improved performance.

Insert #1 was made from porous tungsten matrix filled with 20% by weight silver. The assay sheet of the infiltrated insert as provided by the vendor is shown in Table III-1.

Insert #2 was machined from a solid tungsten forging.

Insert #4 was made as shown on Figure III-1 except that the vent holes were milled rather than drilled. The tungsten cap in the required thickness was applied by a hot chemical plating process by San Fernando Laboratories of Pacoima, California. The coating was crack free, metallurgically bonded to the tungsten-silver substrate and 100% theoretical density. The silver content of the substrate was not affected by the plating process.

The inserts were assembled into test nozzles and were ready for testing.

IV-2 Test Firing Conditions and Results

The nozzles with Inserts #1 and #2 were fired at Langley Research Center in October, 1966. The test nozzle with the encapsulated Insert #4 was fired at Langley Research Center in January, 1967. Firing conditions for all five test inserts are shown in Table IV-1.

TABLE IV-1

Test Summary

	Insert #1 Unencapsulated Silver Impregnated Tungsten (Control	Insert #2 Solid Tungsten Forging (Control)	Insert #3 Plasma Spray Encapsulated Silver Impregnated Tungsten	Insert #4 Chemical Plating Encapsulated Silver Impregnated Tungsten	Insert #5 Chemical Plating Encapsulated Silver Impregnated Tungsten with Longitudinal Gas Passages and Milled Downstream Vent
Fuel Flow #/sec	2.62	2.43	1.97	1.57	3.38
Oxidizer Flow #/sec	3.72	3.80	3.19	3.75	3.80
Pressure PSIA	765	715	500	715	755
Temperature °F	6760	6830	6700	6740	6850
Figure of Merit-Seconds	28	24	29.3	31.5	16.5
Total Firing Time	30	25	39.6	Not Recorded	17.5

Firing pressure traces of Inserts 1 and 2 are shown on Figures IV-1 and IV-2

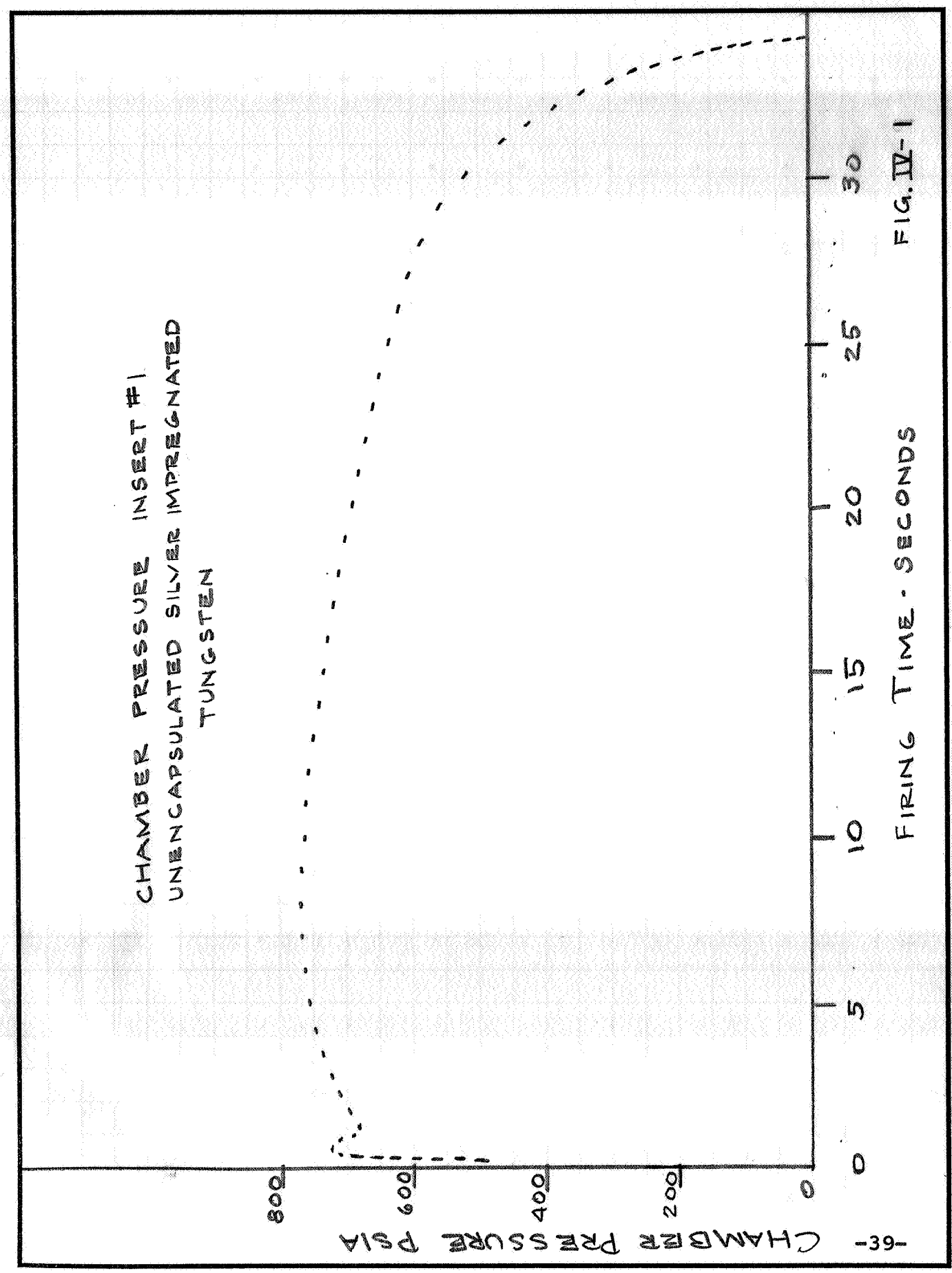
CHAMBER PRESSURE INSERT #1
UNENCAPSULATED SILVER IMPREGNATED
TUNGSTEN
CHAMBER PRESSURE PSIA
800
600
400
200
0
FIRING TIME - SECONDS
0
5
10
15
20
25
30

FIG. IV-1

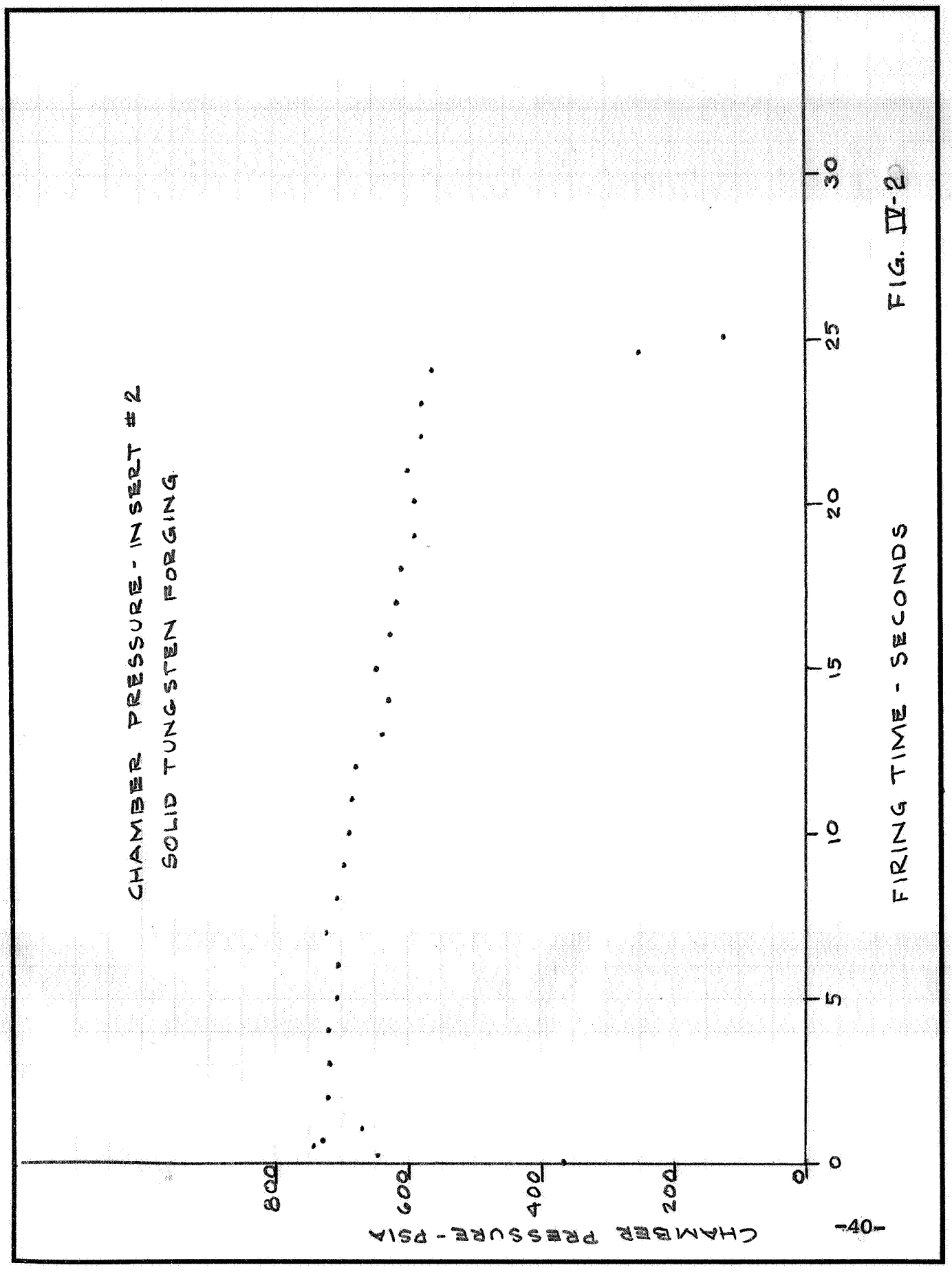
CHAMBER PRESSURE - INSERT #2
SOLID TUNGSTEN FORGING
CHAMBER PRESSURE - PSIA
800
600
400
200
0
FIRING TIME - SECONDS
0
5
10
15
20
25
30

FIG. IV-2

The Figure of Merit (FOM) is taken as the firing time before the chamber pressure drops to 79% of the initial stable pressure.

The firing conditions were reasonably close to the design conditions.

To make the nozzle performance comparison meaningful, the test managers made every effort to ensure uniform firing conditions for each of the three nozzles. These efforts were not completely successful and the firing conditions varied from test to test. Nozzle #2 was exposed to a higher temperature than the others; Nozzle #1 was subject to a higher pressure than the others, and the fuel flow with Nozzle #4 was much less than for either #1 or #2.

Looking at the raw figures of merit, Insert #4 performed slightly better than Insert #1; however, since Insert #4 was exposed to a lower firing pressure than Insert #1, there is a question whether the higher FOM is due to the virtues of Insert #4, or to the slightly less severe firing conditions sustained by Insert #4. The FOM for Insert #2 was considerably less than for either #1 or #4. Although the firing temperature for #2 was higher than for #1 or #4 this fact was offset at least with reference to Insert #1 by a lower chamber pressure.

The figures of merit indicate a slight performance superiority for the encapsulated Insert #4. This indication is blurred by the variations in firing conditions between tests so that while the FOM indicates the encapsulated #4 insert is better than its rivals this is not enough to prove a decisive superiority.

IV-3 Post Fire Analysis of Encapsulated Insert #4

Insert #4 was sectioned, polished and etched for metallurgical examination. Figure IV-3 shows a full scale drawing of the insert cross section. One notes immediately that most of the tungsten cap on the downstream nozzle surface and some of the cap on the upstream nozzle surface survived the firing. This is in contrast to the condition of Insert #3 where the plasma spray deposited tungsten cap was completely wiped off. We can conclude that the chemically plated tungsten coat on Insert #4 was substantially stronger than the plasma sprayed coating on Insert #3.

Microscopic examination of the section indicated that the silver infiltrant had evaporated from the porous tungsten substrate only in the vicinity of openings in the tungsten cap. Thus we see a silver depleted area around the vent grooves near the nozzle exit and two other depleted areas around upstream insert regions where the tungsten cap had been

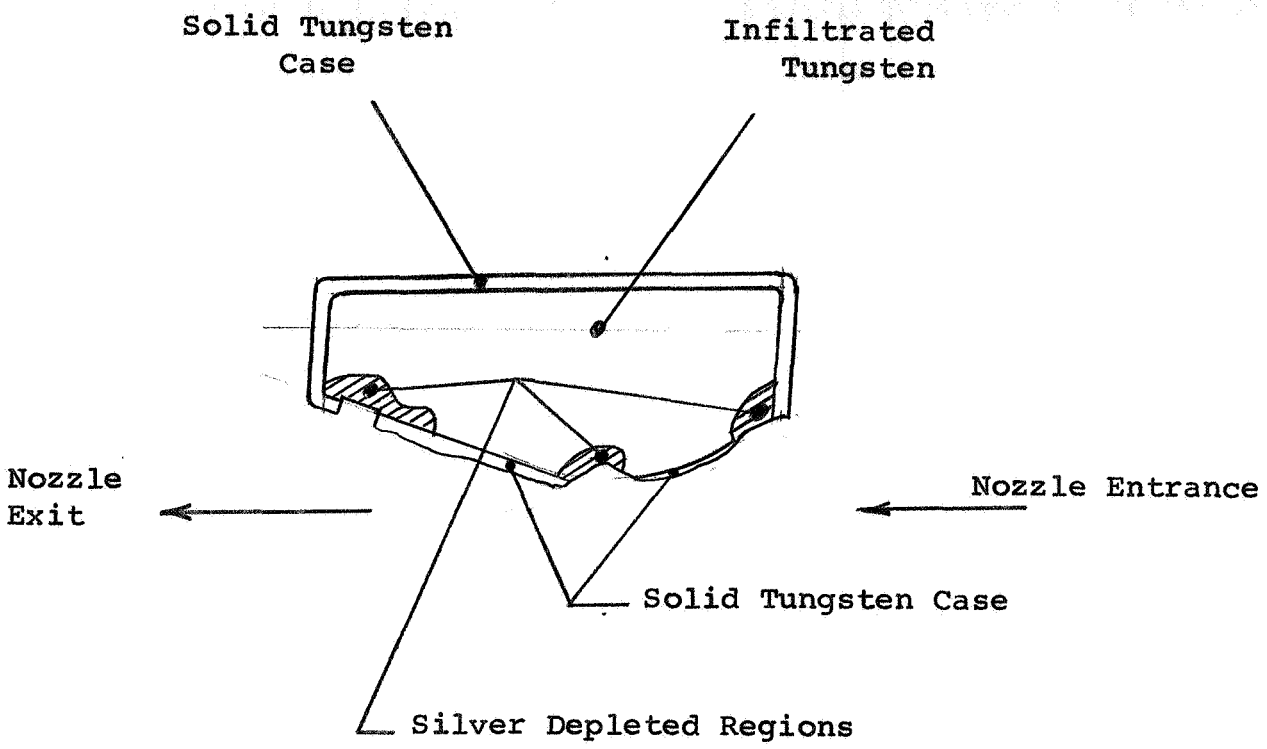

CROSS SECTION OF FIRED ENCAPSULATED NOZZLE INSERT #4

Figure IV-3

eroded away by the propellant gases. These observations indicate that the silver infiltrant will evaporate only near a vent point. During firing only the portion of the insert near the venting groove benefited from evaporative cooling; the rest of the insert behaved as an ordinary solid tungsten insert until part of the upstream cap had eroded away at which time this portion of the nozzle began to behave like an unencapsulated infiltrated insert.

Insert #4 had been designed on the assumption that as soon as the substrate in the insert throat region reached 5000°F, silver vapor at 150 psi would be generated, and would find its way to the exit vent (Section III-1.2). The post firing analysis shows this did not occur; the design of Insert #4 was not correct in that it did not permit evaporative cooling of the insert anywhere except near the vent. The firing of Insert #4 thus did not produce a true test of the basic encapsulation and preferential venting concept.

V - INSERT #5

V-1 Description

The results of the test on Insert #4 showed that the upstream regions of the insert must have free access to the downstream vent groove to permit evaporative cooling. The design of Insert #5, as shown on Figure V-1, provides open longitudinal passageways in the nozzle insert just below the tungsten cap. The passageways are so distributed that all parts of the substrate-cap interface of the insert are within 1/8" of an open groove leading to the downstream vent. 1/8" is slightly less than the silver migration distance noted in post firing examination of Insert #4.

As with Insert #3 and Insert #4, the vent was located 1 1/4" downstream of the insert throat. At this point, as before, the pressure ratio is .118, and the anticipated vent pressure is 89 psia corresponding to a silver vaporization temperature of 4750°.

A detailed thermal analysis of the insert throat section was performed which indicated that the highest temperature to be expected on the gas side surface at the throat of the insert would be 5236°F if the evaporating silver cooled the tungsten cap as envisaged by the encapsulation theory.

REVISIONS				
ZONE	LTR	DESCRIPTION	DATE	APPROVED

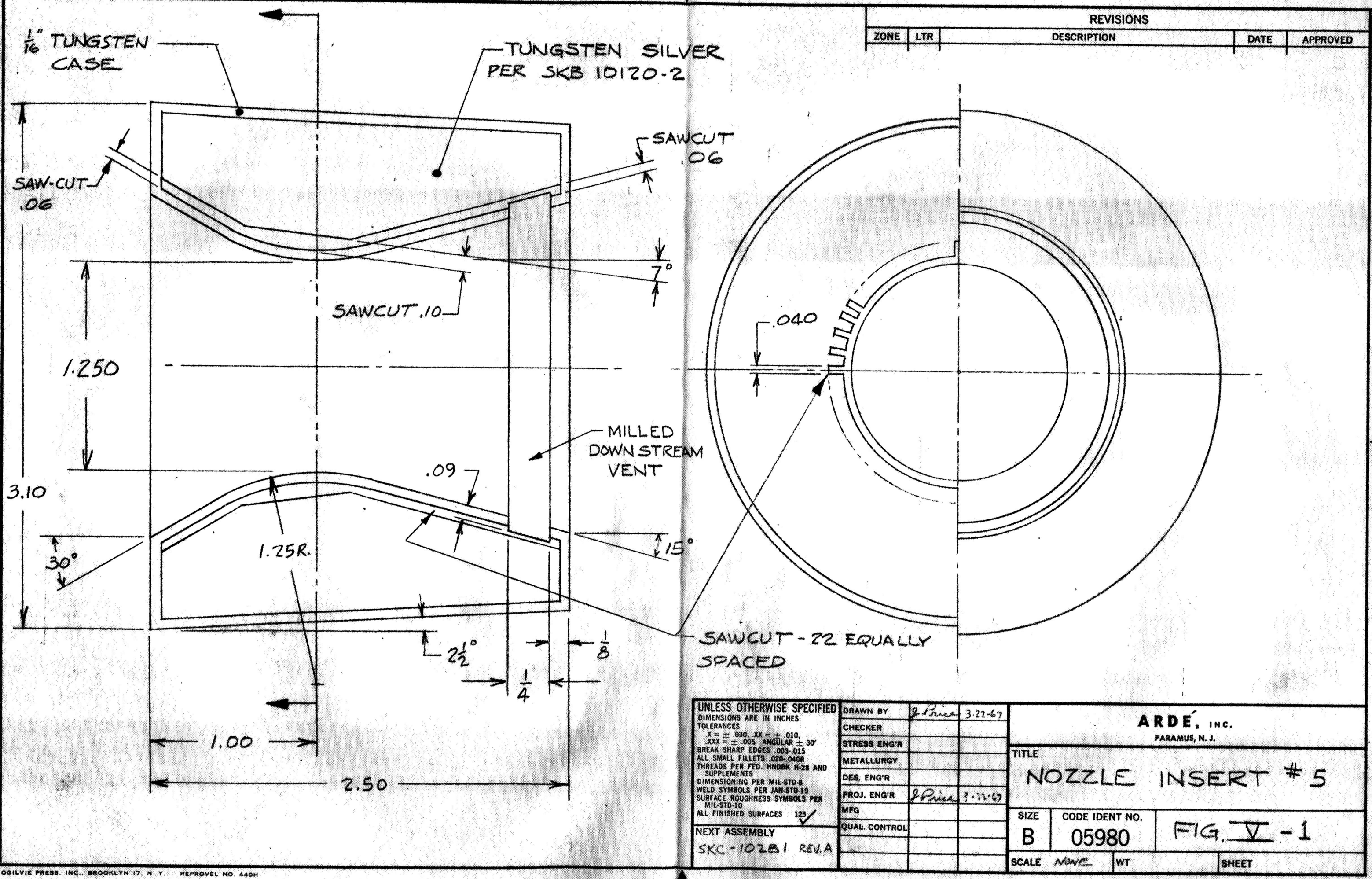

UNLESS OTHERWISE SPECIFIED			
DIMENSIONS ARE IN INCHES TOLERANCES X = ± .030, XX = ± .010, .XXX = ± .005 ANGULAR ± 30' BREAK SHARP EDGES .003-.015 ALL SMALL FILLETS .020-.040R THREADS PER FED. HNDBK H-28 AND SUPPLEMENTS DIMENSIONING PER MIL-STD-8 WELD SYMBOLS PER JAN-STD-19 SURFACE ROUGHNESS SYMBOLS PER MIL-STD-10 ALL FINISHED SURFACES 125 ✓			
NEXT ASSEMBLY SKC-10281 REV. A	DRAWN BY	J. Price	3-22-67
	CHECKER		
	STRESS ENG'R		
	METALLURGY		
	DES. ENG'R		
	PROJ. ENG'R	J. Price	3-22-67
	MFG		
	QUAL. CONTROL		

ARDÉ, INC.
PARAMUS, N. J.

TITLE
NOZZLE INSERT # 5

SIZE	CODE IDENT NO.	
B	05980	FIG. V-1

SCALE NONE | WT | SHEET

OGILVIE PRESS, INC., BROOKLYN 17, N. Y. REPROVEL NO. 440H

V-2 Test Conditions and Test Results

Insert #5 was fired at Langley Research Center on October 4, 1968 under the following conditions:

Fuel flow	3.38 lbs/sec
Oxidizer flow	3.80 lbs/sec
Pressure	755 psia mean stable pressure
Figure of merit-seconds	16 1/2
Temperature °F	6850°

The system fired smoothly for 10 seconds. At that time a shower of sparks issued from the nozzle, and the chamber pressure began to drop off rapidly indicating rapid throat erosion. Six and one half seconds later, the chamber pressure had dropped 25% from 755 psia to 565 psia and the test was terminated. The pressure trace is shown on Figure V-2.

Examination of the fired insert showed that the tungsten cap on the gas side of the insert was completely peeled away revealing the longitudinal vapor grooves.

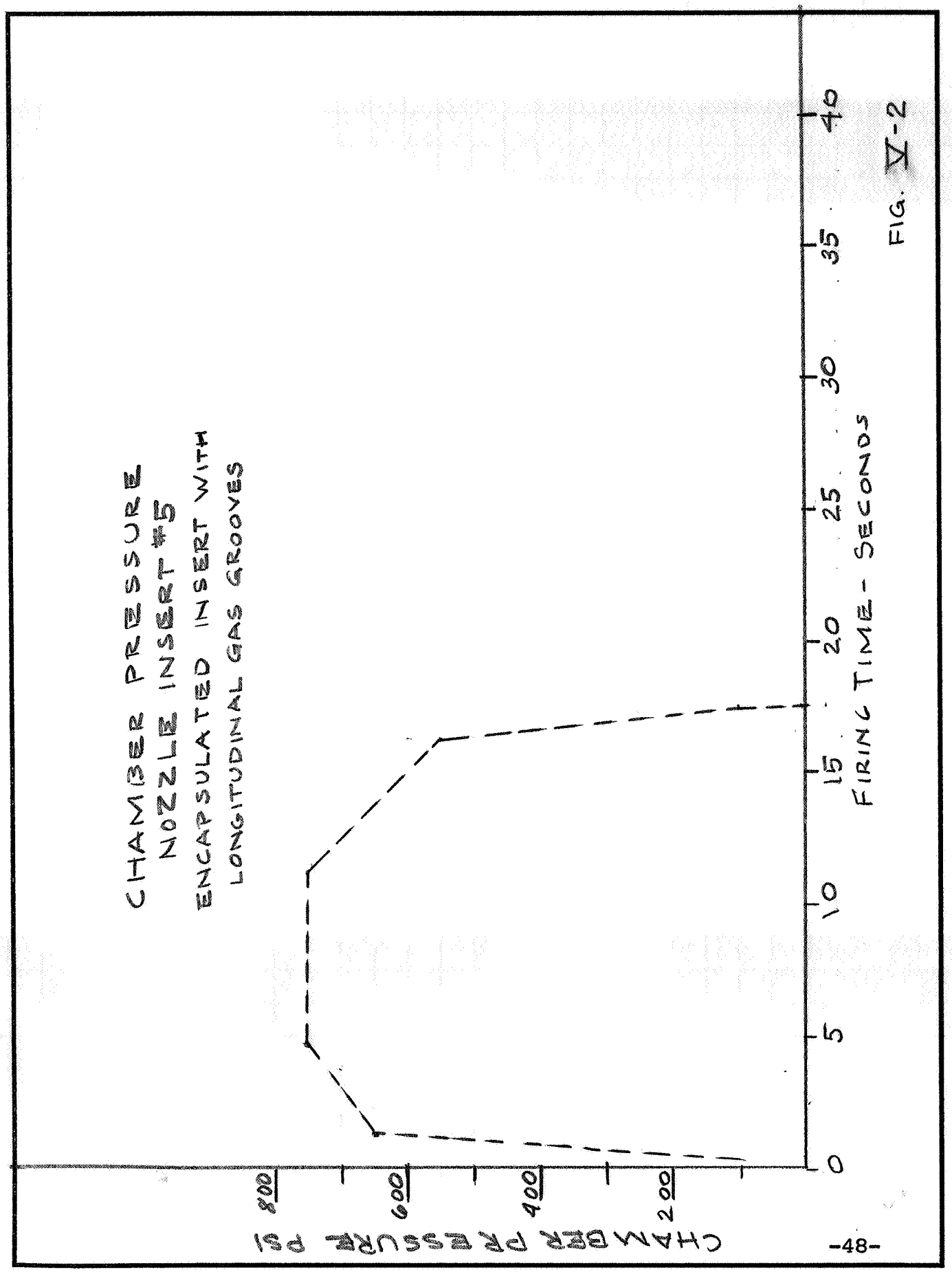
CHAMBER PRESSURE
NOZZLE INSERT #5
ENCAPSULATED INSERT WITH
LONGITUDINAL GAS GROOVES
CHAMBER PRESSURE PSI
800
600
400
200
0
5
10
15
20
25
30
35
40
FIRING TIME - SECONDS

FIG. V-2

VI - CONCLUSIONS AND RECOMMENDATIONS

The tests described in this Final Report have not succeeded in demonstrating the validity of the encapsulation theory or the value of encapsulating nozzle inserts. Based on overall performance, encapsulated inserts performed only marginally better, or considerably worse than unencapsulated inserts. Post firing examination of Insert #4 proved that there was no silver evaporation remote from a vent. Examination of the grooved Insert #5 sheds no light on whether there was evaporative cooling of the cap since the entire cap peeled off during the test. In any case, whatever cooling may have occurred with Insert #5 was ineffective. Failure to obtain migration of the encapsulated silver appears to be a common underlying cause of premature failure of the encapsulated nozzles.

The one point open to question is whether the combination of processes required to groove and cap Insert #5 weakened either the tungsten cap or the adhesion of the cap to the substrate and thus contributed to rapid failure of the cap. At this time, however, the question is academic since the processes used are the best currently available.

In accordance with the program objective, as stated on Page 2, it is recommended that the test results be utilized to establish, by continued development effort, a more appropriate design and/or manufacturing technique for meeting the projected high temperature performance requirements for solid propellant rocket nozzles.

VII - REFERENCES

1. Perez, M.
"Optimum Utilization of Impregnated Throat Inserts in Rocket Nozzles by Surface Encapsulation and Preferential Venting"
Presented American Institute of Aviation and Astronautics Solid Propellant Rocket Conference January 1964

2. Carus, H.
"Numerical Techniques for the One Dimensional Heat Conduction Equation"
Arde Associates 1955

3. Dusinberre, G.M.
"Numerical Analysis of Heat Flow"
McGraw-Hill 1949

4. Gessner, F.B.
"Analysis of Self-Cooling with Infiltrated Porous Tungsten Composites"
Journal of Spacecraft Vol. 1, No. 6 November-December 1964

APPENDIX 1

ANALYSIS OF VAPOR FLOW IN AN ENCAPSULATED INSERT

In order to determine the pressure distribution within the porous matrix of an encapsulated insert it is necessary to consider the flow of the vapors generated by the vaporizing liquid coolant, during heating.

During the initial heating of the insert, the coolant, which is at first solid, liquefies and expands as its temperature increases. The coolant near the surface then begins to vaporize and pressure is built up between the impermeable cap and the liquid coolant below, causing a vapor filled gap to form between the cap and liquid. This condition is shown schematically below; as represented by a one-dimensional model.

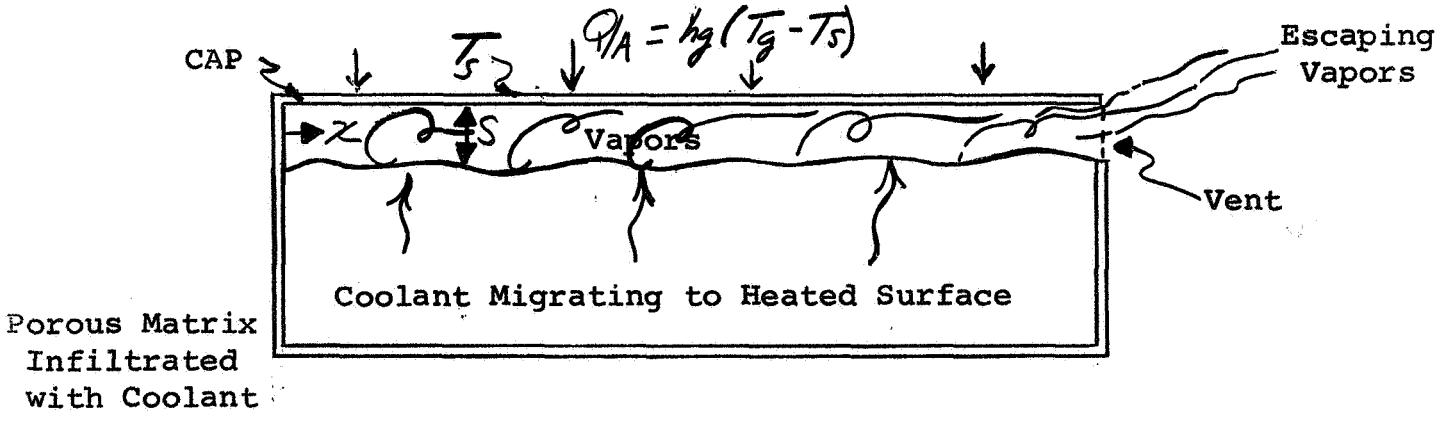

ONE-DIMENSIONAL MODEL FOR VAPOR FLOW

It will be assumed, on the basis of experiments performed with silver impregnated tungsten, that the silver migrates to the surface as quickly as it is consumed, which will then lead to the following boundary conditions for the model proposed:

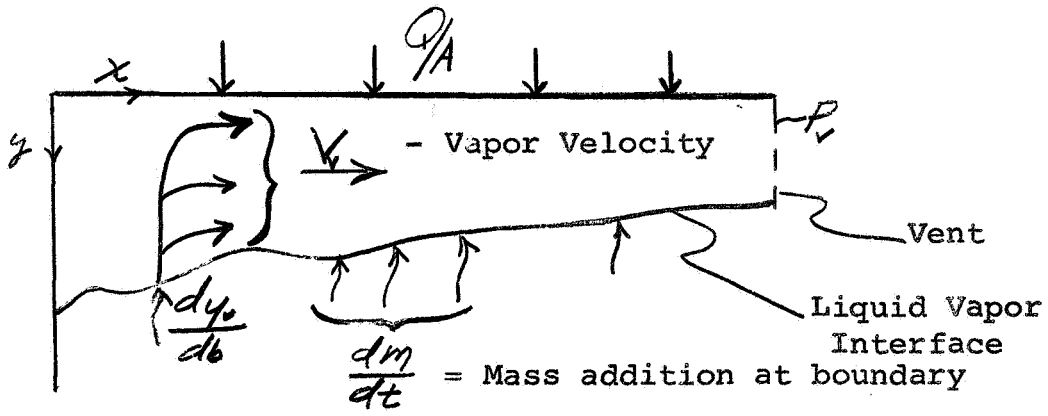

Where:

$Q/A = Q/A\ (x)$ Heat Flow per unit area

$P = P\ (x)$ Pressure of vapor

$V_v = V_v\ (x)$ Velocity of vapor

$S = S\ (x)$ Gap width for flow of vapors

$\frac{dm}{dt} = M$ rate of mass addition at boundary

The flow of the coolant vapors in the porous gap (S) can be described by Darcy's law:

$$\vec{V} = -\nabla\left(\frac{k}{\mu}P\right) \qquad (1)$$

where $\vec{V}$ is a superficial velocity (Reference B-1) based on the area to which the vapors are exposed (S). For a one-dimensional case, and assuming constant properties:

$$\frac{k_g}{\mu} = K \text{ a constant}$$

$$\therefore \quad V_x = -K(dp/dx)$$

but the actual velocity of the vapors (Vg) is given by (Reference B-1).

$$V_v = \frac{V_x}{P}$$

where P is the matrix porosity

$$\text{then } V_v = \frac{-K}{P} \frac{dp}{dx} \tag{2}$$

considering a differential element

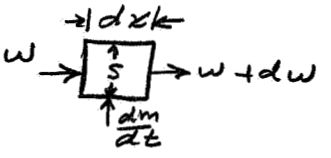

by continuity (for steady state)

$$w + dw = w + \frac{dm}{dt}$$

$$\text{or} \quad \frac{dm}{dt} = dw$$

now

$$V_g = w / \rho_v A_x \quad ; \quad A_x = P S (1) \tag{3}$$

but

$$\int_0^w dw = w = \int_0^x dm/dt$$

but $\frac{dm}{dt}$, the mass addition at the boundary is given by the amount of silver vaporized which is found from an energy balance:

$$dQ = U(T_g - T_v)\,dA_s = \rho_\ell \frac{(dVol)_\ell}{dt} L_v \qquad (4)$$

where $dA_s = dx$ (1)

but

$$\frac{(dVol)_\ell}{dt} = d/dt\,(dy_v\,dx\,(1)\,\mathcal{P}) = \mathcal{P}\,dx\left(\frac{dy_v}{dt}\right)$$

based on the actual surface area, where the porosity ($\mathcal{P}$) of the matrix corrects the actual surface area A_s to give the volume of coolant.

now $dm = \rho_\ell\,(dVol)_\ell$

then $dm/dt = \dot{m} = \rho_\ell \frac{(dVol)_\ell}{dt}$

substituting this last expression in equation (4)

$$U(T_g - T_v)\,dx = L_v \dot{m} \quad \text{or} \quad \dot{m} = \frac{U(T_g - T_v)\,dx}{L_v}$$

now

$$w = \int_0^x dm/dt = \int_0^x \left(\frac{U(T_g - T_v)}{L_v}\right) dx$$

assuming $(T_g - T_v)$ does not vary greatly (which is approximately true for this application) and using an average thermal conductance ($\bar{U}$)

$$w \simeq \left[\frac{\bar{U}(T_g - T_v)}{L_v}\right] x$$

If this approximation is not made, non-linearities result.

$$\therefore \quad V_v = \frac{w}{\rho_v S \mathcal{P}} = \frac{\bar{U}\,(T_g - T_v)\,dx}{L_v \rho_v S \mathcal{P}}$$

If it is now assumed that the vapor's state is approximated by the perfect gas law, where an average vapor temperature ($\bar{T}_v$) is used,

$$\rho_v \cong P/R\bar{T}_v$$

$$\frac{\bar{U}(T_g - T_v)R\bar{T}_v}{L_v P S \rho} x = V_v \qquad (5)$$

substituting Equation (5) into equation (2) yields:

$$\frac{\bar{U}(T_g - T_v)R\bar{T}_v}{L_v P S \rho} x = -K/\rho\left(\frac{dP}{dx}\right) \qquad (6)$$

or

$$\frac{\bar{U}(T_g - T_v)R\bar{T}_v}{L_v S K} x\,dx = -P\,dP$$

let

$$\frac{\bar{U}R\bar{T}_v}{L_v K} = B \qquad \text{a constant}$$

then

$$B x\,dx = \frac{-S P\,dP}{(T_g - T_v)}$$

The gap widths, related to the flow area, should also vary. The variation is not known at the moment, however it is reasonable to assume that it will vary directly with the pressure. Since it has been observed experimentally that silver will travel to, and actually through a heated surface, it will be assumed that at zero pressure there will be a gap of zero width. Then it is reasonable that the gap width can be expressed by a linear relationship:

$$S = cP$$

Now, since T_v, the vaporization pressure, is a function of pressure, it will be approximated in the region of application as a straight line:

$$T_v \approx mp + b$$

Equation (6) can then be integrated

$$\int_0^x Bx\,dx = \int_p^{P_v} \frac{-SP\,dp}{(T_g - T_v)}$$

the result is:

$$\frac{m^3}{C} B x^2 = (T_g - b)^2 \ln \left| \frac{(T_g - b) - m P_v}{(T_g - b) - mp} \right| - (T_g - b) m (P - P_v) - \frac{1}{2} m^2 (P^2 - P_v^2) \qquad (9)$$

which is seen to be explicit in x, the length of the heated surface.

Rearranging equation (9) and expanding the constant B shows that

$$x^2 = \left(\frac{2 c L_v k_g}{m^3 \mu \bar{U} R \bar{T}_v} \right) \left[f(P_v, P) \right]$$

which shows that L, the maximum length of an encapsulated insert will be proportional to:

$$L \propto \sqrt{\frac{2 c L_v k_g}{m^3 \mu \bar{U} R \bar{T}_v}}$$

for a given maximum allowable pressure and vent pressure (P_v).

In order to increase the allowable length (L) of an encapsulated insert the following parameters can be varied.

1. $\bar{U}$ - The average thermal conductance could be reduced by reducing the nozzle throat heat transfer coefficient or increasing the cap thickness.

   where $$\bar{U} = \frac{1}{\frac{1}{\bar{h}_g} + \frac{t_c}{K_c}}$$

   and t_c = cap thickness

   K_c = cap thermal conductivity

   and $\bar{h}_g$ = average gas side heat transfer coefficient.

2. L_v - can be increased by choosing a coolant with a high heat of vaporization.

3. k - The permeability can be increased by choosing a matrix with a high permeability.

4. μ - The viscosity of the coolant vapor can be made small by the proper choice of coolant.

The importance of equation (9) lies in its ability to predict the important parameters and the magnitude of their effect on the pressures within the porous matrix.

Equation (9) should also result in a first order estimate of the actual pressure distribution within the insert, particularly if some of the approximated constants are further refined.

NOMENCLATURE

A - Area

B - A constant defined in equation (7)

b - A constant

c - Constant relating gap size to pressure

g - units conversion constant-$32.2 \frac{lb_m - ft}{lb_f - sec^2}$

h_g - nozzle gas side heat transfer coefficient

K - Constant ($\frac{kg}{\mu}$)

k - Permeability

L_v - Latent heat of vaporization

m - Approximate slope of vapor pressure curve

p - Pressure

φ - Porosity

Q - Heat flux

R - Gas constant

S - Gap width for vapor flow below gap

T - Temperature

t - time

U - Thermal conductance between nozzle exhaust gases and coolant

V - Velocity of coolant vapors.

Vol - Volume

x - Coordinate in direction of vapor flow

y - Coordinate normal to vapor flow.

y_v - Location of coolant liquid vapor interface

μ - Viscosity of coolant vapors

w - Mass flow rate of vapors

SUBSCRIPTS

g - Refers to hot exhaust gas side of cap

l - Refers to liquid coolant

x - Refers to x direction

v - Refers to coolant vapors below cap and vent location

REFERENCES

B-1 - Scheidegger, A. E., "The Physics of Flow Through Porous Media", University of Toronto Press, 1960.

B-2 - Owen, L. and Cliffel, E., "Development of Refractory Materials for Rocket Nozzles and Vanes", Summary Report, Sept. 1, 1961 through Aug. 31, 1962. Contract NOrd 18887, Confidential.

APPENDIX 2

CALCULATION OF INSERT THROAT TEMPERATURES

Throat temperatures were calculated on a one dimensional basis. This means that the temperature at any point in the throat cross section shown on Figure 2-1 was assumed to be a function only of its radial distance, R, from the axis of the throat and the elapsed time of firing. Heat flow parallel to the nozzle axis is assumed to be negligible.

For the calculation performed, the gas temperature Tg was taken at 6855°F, the convective coefficient of heat transfer from the hot gas to the throat, hg, was calculated to be 1674 BTU/hr ft^2 °F. The effective heat transfer coefficient from the hot gas to the tungsten silver matrix was calculated from the formula

$$h_{effective} = \frac{hg}{1+\frac{hg\,s}{k}} = 1469 \text{ BTU/hr } ft^2 \text{ °F}$$

where s = thickness of tungsten cap = .062"

k = thermal conductivity of tungsten
= 62.5 BTU/hr ft °F (See Table III-2)

The vaporization temperature of silver was taken as 5000°F corresponding to a pressure of 150 psia. The latent heat of fusion of silver is 40 BTU/lb, the heat of vaporization is 900 BTU/lb at 150 psi. The heats of vaporization and fusion were combined for a total of 940 BTU/lb for solid to vapor phase change. For the 80% tungsten 20% silver insert the volumetric heat of vaporization plus fusion is 123,000 BTU per cubic foot.

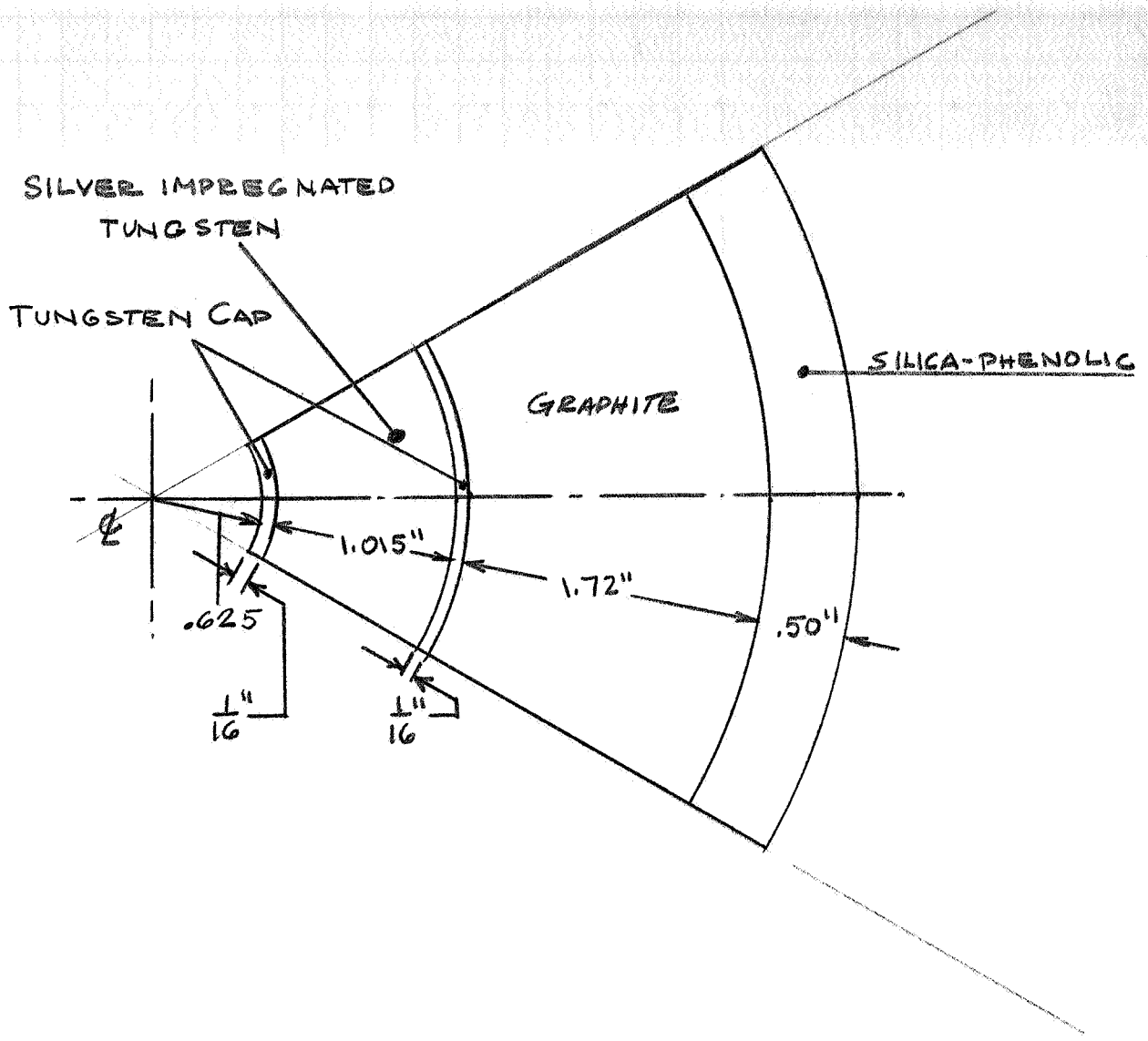

NOZZLE THROAT CROSS-SECTION

FIG. 2.1

For purposes of calculation the silver tungsten matrix was divided into 12 annuli of equal thickness the graphite into 24 annuli of equal thickness and the silica phenolic into 5 annuli of equal thickness. Because of its high conductivity, the effect of the tungsten cap between the tungsten silver matrix and the graphite was neglected. Calculation of temperatures were then carried out in accordance with the methods of References 2 and 3. For example, consider point 0 at one of the annular interfaces in the tungsten silver matrix, see Figure 2-2. The temperature To' of Point 0 after the elapse of time Δt is--

$$To' = \frac{\alpha \Delta t}{h^2}\left(1 - \frac{h}{2Ro}\right) T_{-1} + \left(1 - \frac{2\alpha \Delta t}{h^2}\right) To$$

$$+\frac{\alpha \Delta t}{h^2}\left(1 + \frac{h}{2Ro}\right) T_{+1} \quad \text{(Ref. 2 Equation 11 Also Ref.3)}$$

where α = diffusivity of the tungsten silver matrix

Ro = radial distance of Po from nozzle axis

h = annular thickness

and T_{-1}, To, and T_{+1} are the initial temperatures of points P_{-1}, Po and P_{+1} respectively.

Starting with an initial temperature of 100°F at every point in the cross section, 6855°F gas temperature and a time increment of Δt = .05 seconds, the temperature of every point can be determined after any number of time increments by repeated application of the foregoing equation at each point. References 2 and 3 provide special equations for points at the nozzle throat surface and for points at the interfaces between different materials. At the nozzle throat surface the equation to be used is--

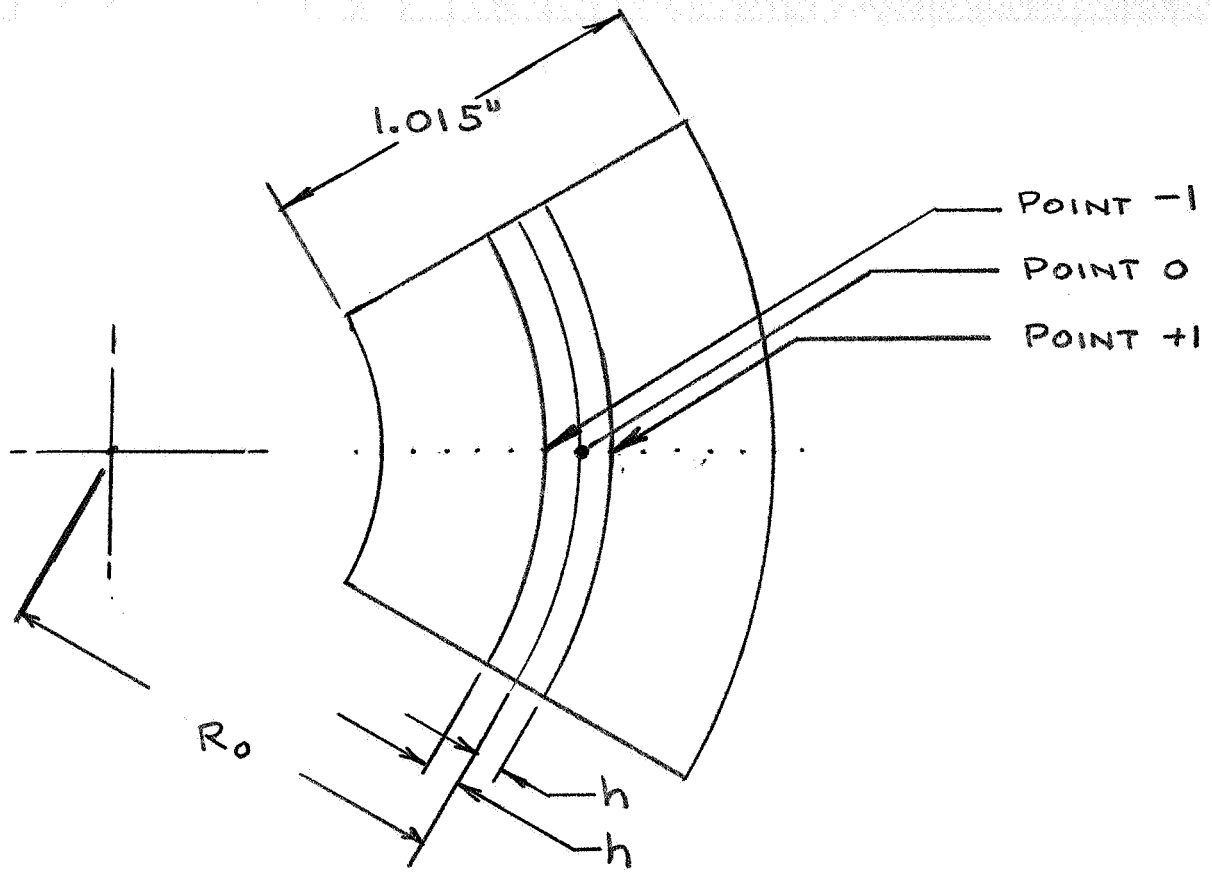

HEAT FLUX IN TUNGSTEN SILVER MATRIX

FIG. 2.2

$$T_o' = 2h_q T_q \left(1-\frac{h}{2R_o}\right)\frac{\Delta t}{\rho c h} + \left[1 - \frac{2\alpha\Delta t}{h^2} - 2h_q\frac{\Delta t}{\rho c h}\left(1-\frac{h}{2R_o}\right)\right] T_o$$

$$+ 2\frac{\alpha\Delta t}{h^2} T_{+1}$$

where h_g = convective gas side heat transfer coefficient
T_g = gas temperature
h = thickness of annulus
R_o = radius to nozzle surface
Δt = time increment
ρ = density of throat material
c = specific heat of throat material
α = diffusivity of throat material
T_o = initial throat temperature
T_+ = initial temperature at (Roth)

At the interface between two different materials, the equation used is $T_o' = \left(\frac{K_{-1}}{h_{-1}}\frac{\Delta t}{\eta'}\right)T_{-1} + \left[1-\left(\frac{K_{-1}}{h_{-1}}+\frac{K_{+1}}{h_{+1}}\right)\frac{\Delta t}{\eta'}\right]T_o$

$$+\left(\frac{K_{+1}}{h_{+1}}\frac{\Delta t}{\eta'}\right)T_{+1}$$

where: k_{-1} = thermal conductivity of material inside R_o
k_{+1} = thermal conductivity of material outside R_o
h_{-1} = annulus thickness inside R_o
h_{+1} = annulus thickness outside R_o
$\eta' = \frac{1}{2}\left[(\rho c h)_{-1} \div \left(1+\frac{h_{-1}}{2R_o}\right) + (\rho c h)_{+1} \div \left(1-\frac{h_{+1}}{2R_o}\right)\right]$

When the temperature of a point such as Po in the tungsten silver matrix reaches the assumed vaporization temperature 5000°F, this temperature is held constant for a sufficient number of time increments until the heat flux to Po is equal to that required to melt and vaporize the silver in the annulus between Po and P_{+1}. Further details on numerical heat transfer calculation with phase change is given in Reference 4.